ChemPubSoc Europe

DOI: 10.1002/chem.201304419

CHEMISTRY
A European Journal
Full Paper

Olefin Metathesis

Gyroscope-Like Molecules Consisting of PdX_2/PtX_2 Rotators within Three-Spoke Dibridgehead Diphosphine Stators: Syntheses, Substitution Reactions, Structures, and Dynamic Properties

Agnieszka J. Nawara-Hultzsch,[a] Michael Stollenz,[b] Michał Barbasiewicz,[a] Sławomir Szafert,[c] Tadeusz Lis,[c] Frank Hampel,[a] Nattamai Bhuvanesh,[b] and John A. Gladysz*[a, b]

Abstract: Threefold intramolecular ring-closing metatheses of *trans*-[MCl_2(P{$(CH_2)_m$CH=CH_2}$_3$)$_2$] are effected with Grubbs' catalyst. Following hydrogenation catalyzed by [RhCl(PPh_3)$_3$], the title complexes *trans*-[$\overline{MCl_2(P((CH_2)_n)_3\overline{P})}$] ($n = 2m + 2$; M/n = Pt/14, **4c**; Pt/16, **4d**; Pt/18, **4e**; Pd/14, **5c**; Pd/18, **5e**) and sometimes isomers partly derived from intraligand metathesis, *trans*-[$\overline{MCl_2\{P(CH_2)_n(CH_2)_n\}\overline{P}(CH_2)_n)}$] (**4′c–e**, **5′e**), are isolated. These react with LiBr, NaI, and KCN to give the corresponding MBr_2, MI_2, and $M(CN)_2$ species (58–99%). ^{13}C NMR data show that the MX_2 moieties rapidly rotate within the diphosphine cage on the NMR timescale, even at −120 °C. The reaction of **4c** and KSCN gives separable $Pt(NCS)_2$ and Pt(NCS)(SCN) adducts (**13c**, 28%; **14c**, 20%), and those of **4c**,**e** and Ph_2Zn give $PtPh_2$ species (**15c**, 61%; **15e**, 90%). ^{13}C NMR spectra of **13c–15c** show two sets of CH_2 signals (ca. 2:1 intensity ratios), indicating that MX_2 rotation is no longer rapid. Reactions of **4c** or **4′c** and excess NaC≡CH afford the free diphosphines P{$(CH_2)_{14}$}$_3$P (91%) and $(\overline{CH_2)_{14}\overline{P}(CH_2)_{14}\overline{P}(\overline{CH_2)_{14}}}$ (90%). The latter has been crystallographically characterized as a bis(BH_3) adduct. The crystal structures of eight complexes with $P(CH_2)_{14}P$ linkages ($PtCl_2$, $PtBr_2$, PtI_2, $Pt(NCS)_2$, $PtPh_2$, $PdCl_2$, $PdBr_2$, PdI_2) and **15e** have been determined, and intramolecular distances analyzed with respect to MX_2 rotation. The conformations of the $(CH_2)_{14}$ moieties and features of the crystal lattices are also discussed.

Introduction

Macroscopic gyroscopes can assume a number of physical forms,[1] which include biological assemblies, such as the halteres of flying insects.[2] All serve as devices for sensing and/or maintaining the orientation of an object. The classic mechanical gyroscope, encountered by many as a childhood toy, consists of an axle, a "flywheel" that can rotate, and a protective housing. When the object is displaced from its axis of rotation, there is a restoring force arising from the conservation of angular momentum.[3] The underlying physics also holds at the molecular level,[4] allowing chemists to pursue the ultimate limit of gyroscope miniaturization. Many other approaches to microscopic gyroscopes are also receiving attention,[5] driven by a variety of technological applications, the most ubiquitous being mobile-phone display screens.

Molecular gyroscopes constitute one subset of molecular rotors,[4] which are composed of "rotators" and "stators". Since motion associated with a component of any object is a function of the frame of reference, the stator is taken as the subunit with the greater moment of inertia. In a series of communications[6–11] we have described the syntheses of gyroscope-like molecules in which a metal-based rotator, ML_n, is encased in a macrobicyclic dibridgehead diphosphine stator, such that a P-M-P axle or axis results. Full papers that detail related diphosphite- and dipyridine-based systems are also available.[12,13]

As shown in Scheme 1, the diphosphine and diphosphite systems have been accessed by surprisingly effective threefold intramolecular ring-closing metatheses of *trans*-monophosphorus ligands, followed by hydrogenation (**I**→**II**). These sequences can be conducted in trigonal-bipyramidal, square-planar, and octahedral coordination spheres (**III**–**V**). Many elegant studies of purely organic or organosilicon models for molecular gyroscopes, some with similar topologies, have been reported by the Garcia-Garibay[14,15] and Setaka groups.[16,17] The most relevant assemblies are described in the discussion section.

[a] Dr. A. J. Nawara-Hultzsch, Dr. M. Barbasiewicz, Dr. F. Hampel, Prof. Dr. J. A. Gladysz
Institute of Organic Chemistry and
Interdisciplinary Center for Molecular Materials
Friedrich-Alexander-Universität Erlangen-Nürnberg
Henkestrasse 42, 91054 Erlangen (Germany)

[b] Dr. M. Stollenz, Dr. N. Bhuvanesh, Prof. Dr. J. A. Gladysz
Department of Chemistry, Texas A&M University
PO Box 30012, College Station, Texas 77842-3012 (USA)
E-mail: gladysz@mail.chem.tamu.edu

[c] Dr. S. Szafert, Dr. T. Lis
Department of Chemistry, University of Wroclaw
F. Joliot-Curie 14, 50-383 Wroclaw (Poland)

Supporting information for this article is available on the WWW under http://dx.doi.org/10.1002/chem.201304419.

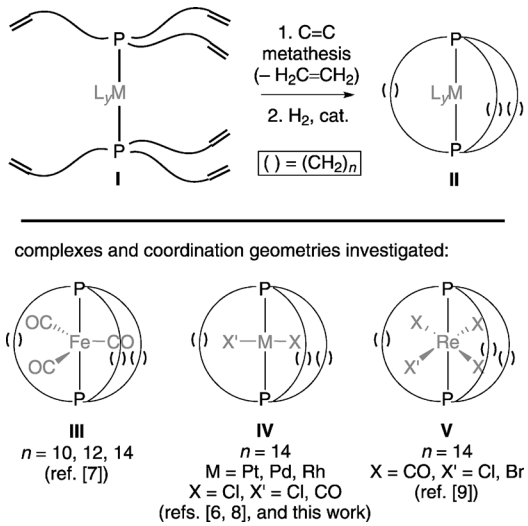

Scheme 1. Syntheses of gyroscope-like complexes based upon *trans*-spanning diphosphines with $(CH_2)_n$ linkers.

In this full paper, we document our initial efforts with gyroscope-like complexes based upon square-planar platinum and palladium cores. The effectiveness of intramolecular ring-closing metathesis is probed as a function of macrocycle size. The feasibility of substitution reactions within the gyroscope cages is then demonstrated. The sizes of the ligands are varied to probe rotational dynamics within the cage, which are compared to analogues with different coordination geometries. A number of crystal structures are determined that provide additional insight, and define constraints on rotation in the solid state. A small portion of this work has been communicated,[7] and additional details have been described elsewhere.[18]

Results

Gyroscope-like complexes from dichloride complexes

Platinum and palladium dichloride complexes of the formula *trans*-$[MCl_2(P\{(CH_2)_mCH{=}CH_2\}_3)_2]$ ($m = 4$–8) were prepared by routine procedures described previously.[19] [Note that the notation **a**–**e** in the compounds numbers given hereafter, refer to $m = 4$–8, respectively.] The complexes with six methylene groups in each phosphine substituent, *trans*-**1c** (M = Pt) and *trans*-**2c** (M = Pd), were used for lead experiments throughout this study. As shown in Scheme 2, solutions of compounds *trans*-**1c** and *trans*-**2c** in CH_2Cl_2 (0.0035 M) were slowly treated with solutions of Grubbs' catalyst. For all metatheses, catalyst loadings (here 3 and 14 mol% (two charges)) and reaction times were initially optimized by assaying aliquots by NMR spectroscopy.[20] When the $=CH_2$ ^{1}H NMR signals of the reactants were no longer detectable, the mixtures were filtered through alumina.[21] The filtrates were treated with hydrogen (5 bar) in the presence of Wilkinson's catalyst (13–14 mol%). Chromatographic workups gave the target gyroscope-like molecules derived from threefold intramolecular and interligand metatheses, *trans*-**4c** and *trans*-**5c**, in 43 and 36% yields, respectively.

Complexes *trans*-**4c** and *trans*-**5c**, which feature 17-membered macrocycles with 14 methylene groups, were initially obtained as pale yellow waxy oils that solidified with time. Crystals of each could be grown, and the structures were confirmed crystallographically as described below. These and all other gyroscope-like complexes below were stable in air for extended periods of time. They were characterized by NMR (^{1}H, ^{13}C, ^{31}P) and IR spectroscopy, and in most cases by microanalyses, DSC, and mass spectrometry (Experimental Section).

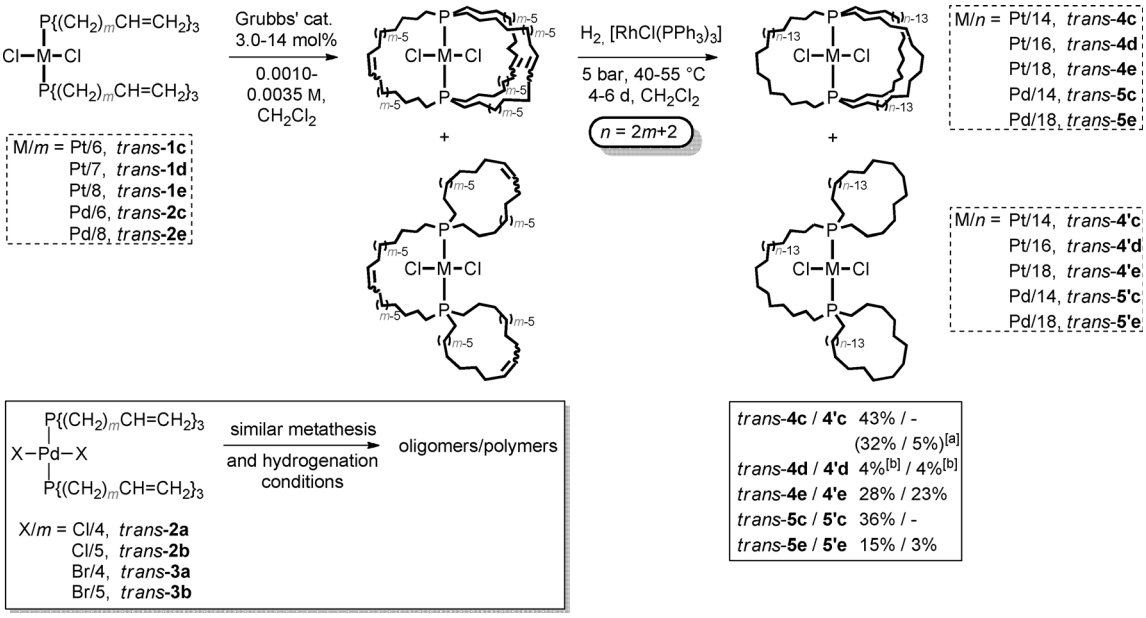

Scheme 2. Metathesis/hydrogenation sequences involving complexes of the formulae *trans*-$[MX_2(P\{(CH_2)_mCH{=}CH_2\}_3)_2]$. [a] Larger scale reaction (see text). [b] Yields from different experiments.

Table 1. Selected $^{31}P\{^1H\}$ and $^{13}C\{^1H\}$ NMR data ($CDCl_3$).

	$^{31}P\{^1H\}$ δ [ppm]	$^{13}C\{^1H\}$ δ [ppm]		
		PCH_2	PCH_2CH_2[c]	$PCH_2CH_2CH_2$
	$[^1J_{PPt}$, Hz][a]	$[^1J_{PC}$, Hz][b]		$[^3J_{PC}$, Hz][b]
trans-**1c**	5.2 [2381]	21.5 [16.2]	24.2	31.5 [6.2]
trans-**1d**	5.2 [2380]	20.4 [16.0]	23.6	31.1 [6.5]
trans-**1e**	5.1 [2381]	20.4 [16.1]	23.6	31.1 [6.3]
trans-**4c**	7.1 [2398]	21.3 [16.3]	23.1	30.0 [6.8]
trans-**4d**	6.0 [2398]	20.8 [16.2]	23.2	31.4 [6.7]
trans-**4e**	6.5 [2389]	20.7 [16.2]	23.4	30.7 [6.6]
trans-**5c**	13.3	22.4 [12.2]	23.5	30.2 [6.7]
trans-**5e**	10.1	21.7 [13.1]	23.9	30.8 [6.6]
trans-**4′c**	5.6 [2374]	23.1 [16.3]	21.7[e]	31.3 [7.3]
		18.9 [15.9][d]		29.0 [6.2][d]
trans-**4′d**	5.5 [2374]	22.8 [16.1][f]	22.6[e]	31.6 [7.2]
		19.2 [16.0][d]		29.9 [6.3][d]
trans-**4′e**	5.4 [2374]	22.6 [16.5][f]	22.8[e]	31.4 [6.8]
		19.3 [16.0][d]		30.6 [6.2][d]
trans-**5′e**	11.0	23.2[g]	25.1[e]	31.5 [7.0]
		20.5 [12.8][d]		30.6 [6.1][d]
trans-**11c**	9.2 [2166]	24.9 [17.2]	23.7	29.8 [7.0]
trans-**11e**	6.8 [2152]	24.7 [17.3]	24.1	30.5 [6.9]
trans-**12c**	17.4	25.7 [14.3]	24.0	30.0 [7.0]
trans-**15e**	3.2 [2807]	21.6 [17.3]	27.8	30.3 [7.0]

[a] Singlets; the platinum complexes exhibit ^{195}Pt satellites (d). [b] Virtual triplets for which the $^1J_{PC}$ values represent the apparent coupling between adjacent peaks. [c] Singlets. [d] Downfield/upfield signals about 1:2. [e] The PCH_2CH_2 signal for the phosphacycle cannot be definitively assigned from present data. [f] One line of this triplet is obscured. [g] Due to overlapping signals, this coupling can only be bounded as between 12 and 15 Hz.

Key NMR data are summarized in Table 1. All complexes exhibited a single $^{31}P\{^1H\}$ NMR signal. The platinum adducts showed ^{195}Pt satellites, the magnitudes of which were consistent with *trans*-P-Pt-P linkages.[22] The ^{13}C NMR spectra exhibited seven ($m+1$ or $n/2$) methylene signals. COSY experiments ($^1H,^1H$ and $^1H,^{13}C\{^1H\}$) with *trans*-**4c** allowed the PCH_2, PCH_2CH_2 and $PCH_2CH_2CH_2$ ^{13}C and ^1H NMR signals to be assigned.[20] Parallel assignments were made for the other complexes. The ^{13}C PCH_2 and $PCH_2CH_2CH_2$ signals were virtual triplets with J values of 17.3–12.2 Hz and 7.0–6.2 Hz, respectively.[23] In contrast, the PCH_2CH_2 signals were singlets.

Similar sequences were conducted with complexes with two additional methylene groups in each phosphine substituent (*trans*-**1e** and *trans*-**2e**). Now, as shown in Scheme 2, appreciable amounts of two types of monometallic metathesis products were obtained. In the case of platinum complex *trans*-**1e**, the gyroscope-like complex *trans*-**4e** with 21-membered macrocycles (eighteen methylene groups) was isolated in 28% yield. The structure followed from its NMR properties, as well as the crystal structure of a derivative below. However, a more polar substance, *trans*-**4′e**, was also isolated in 23% yield. It exhibited two sets of nine ($n/2$) ^{13}C NMR signals in an approximate 2:1 intensity ratio. The mass spectrum showed a molecular ion identical to that of *trans*-**4e**. Accordingly, it was assigned an isomeric structure derived from a combination of inter- and intraligand metathesis, as shown in Scheme 2. This assignment was supported by a crystal structure derived from a homologue, as described below. In the case of palladium complex *trans*-**2e**, the corresponding complexes *trans*-**5e** and *trans*-**5′e** were obtained in lower yields (15 and 3%, respectively).

Comparable sequences were conducted with a platinum complex with seven methylene groups in each phosphine substituent, *trans*-**1d**. However, the yields of monoplatinum complexes were lower, and the composition varied in different runs. In one case, only the gyroscope-like complex *trans*-**4d** was isolated (4%). In another, the isomer *trans*-**4′d** dominated (4%). Reactions were also conducted with palladium dichloride complexes with four or five methylene groups in each phosphine substituent (*trans*-**2a**,**b**). As shown in Scheme 2 (bottom), insoluble powders or gums that were presumed to be oligomers or polymers were obtained. There was no evidence for significant quantities of monopalladium products, even when Grubbs' second-generation catalyst was employed. The exact conditions utilized are detailed elsewhere.[18]

Gyroscope-like complexes from dibromide complexes

Metathesis/hydrogenation sequences were also conducted with analogous palladium dibromide complexes.[19] With *trans*-**3a**,**b**, which feature four or five methylene groups in each phosphine substituent, oligomers or polymers were again obtained (Scheme 2, bottom).

The results with *trans*-**3c** are depicted in Scheme 3. Metathesis was slower than with dichloride analog *trans*-**5c**, and 20 mol% of Grubbs' catalyst was employed. Subsequent hy-

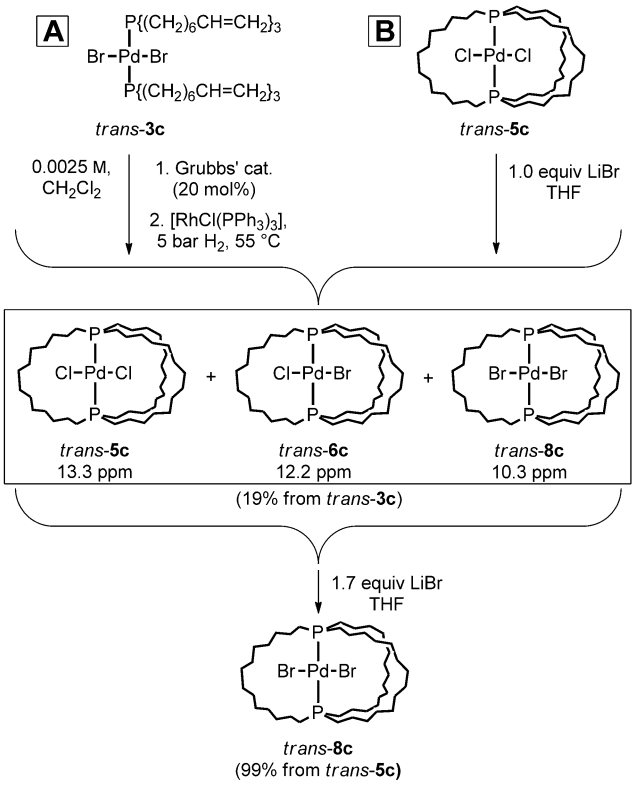

Scheme 3. Metathesis/hydrogenation and substitution sequences leading to the gyroscope-like palladium dibromide complex *trans*-**8c**.

drogenation gave a mixture of three monoplatinum complexes, as assayed by ^{31}P NMR spectroscopy, in about 19% yield (ca. 50:40:10).[20] These could not be separated chromatographically. Pale yellow plates were obtained from CH_3OH/THF, which a crystal structure and independent synthesis below showed to be the target gyroscope-like dibromide complex *trans*-**8c**. This could be assigned to the ^{31}P NMR signal of intermediate intensity (10.3 ppm). The minor signal had the same chemical shift as the dichloride analogue *trans*-**5c** (13.3 ppm). The mass spectrum of the mixture showed an ion with the mass of the mixed monochloride monobromide complex *trans*-**6c**. Accordingly, this was assigned to the major signal (12.2 ppm). Apparently, the chloride ligands in Grubbs' and/or Wilkinson's catalyst are able to exchange with the bromide ligands of palladium.

These assignments were verified by monitoring an independent reaction of the dichloride complex *trans*-**5c** with LiBr. As shown in sequence B in Scheme 3, one equivalent was initially added, thereby generating the mixture of three complexes obtained by metathesis. Then an additional 1.7 equivalents were added, cleanly generating the dibromide complex *trans*-**8c**. Workup of a similar reaction (below) gave *trans*-**8c** in 99% yield. Additional substitution processes are detailed in the section on subsitution reactions and low-temperature NMR data below.

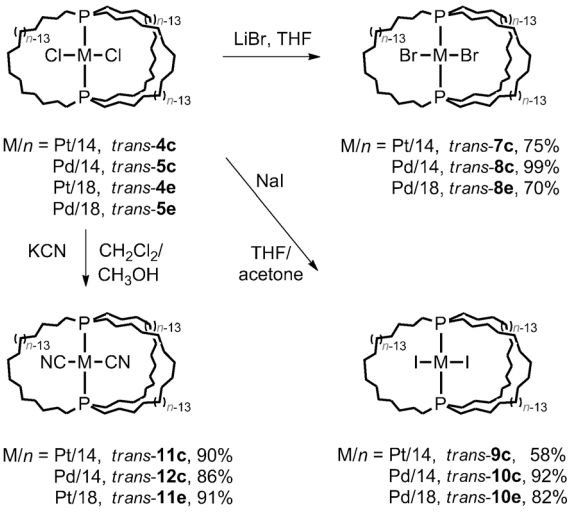

Scheme 4. Substitutions of chloride ligands by bromide, iodide, and cyanide ligands.

Preparative reactions with platinum complex *trans*-1c

Subsequent to the chemistry described above, the platinum dichloride complex *trans*-**4c** became the lead compound for a number of investigations, including studies of a dibridgehead diphosphine obtained below. As such, the sequence with *trans*-**1c** in Scheme 2 has been conducted many dozens of times by many researchers, with the yield of *trans*-**4c** typically slightly greater than 40% on scales up to one gram.

In larger scale reactions, somewhat lower yields of *trans*-**4c** have usually been obtained. A procedure involving five parallel 1.8–2.2 g scale reactions (each 1.0–1.2 L total solvent) and a combined chromatographic workup is given in the Experimental Section. Noteworthy is that, in addition to the 32% yield of *trans*-**4c** isolated, 5% of a new monoplatinum product, *trans*-**4′c**, was obtained (Scheme 2). This species was not detected in the small-scale reactions communicated earlier,[7] although close examinations of NMR spectra of some samples prior to chromatography revealed observable quantities. The structural assignment was supported by a crystal structure of the BH_3 adduct of the free diphosphine ligand, obtained as described below.

Substitution reactions and low-temperature NMR data

The scope of substitution reactions that can be carried out within the diphosphine cages of the gyroscope-like complexes was probed. As shown in Scheme 4, *trans*-**4c** and *trans*-**5c**,**e** were combined with LiBr (2.3–4.0 equiv) in THF at room temperature (homogeneous conditions). Workups gave the corresponding dibromide complexes *trans*-**7c** and *trans*-**8c**,**e**, respectively, as deep yellow powders in 70–99% yields. Similar reactions with NaI (4.0 equiv) in THF/acetone (homogeneous conditions) gave the corresponding orange diiodide complexes *trans*-**9c** and *trans*-**10c**,**e**, respectively, in 58–92% yields. NMR monitoring showed that the palladium complexes underwent complete substitution within 10–20 min, whereas the platinum complexes required hours.

Rotators featuring metal–carbon bonds were also sought. Thus, *trans*-**4c**,**e** and *trans*-**5c** were analogously treated with KCN (2.0–4.0 equiv) in CH_2Cl_2/CH_3OH (homogeneous conditions). Workups gave the dicyanide complexes *trans*-**11c**,**e** and *trans*-**12c**, respectively, as white powders in 86–91% yields. The ^{13}C NMR spectra showed diagnostic signals for the cyanide ligands (124.3–129.5 ppm), which were coupled to phosphorus (t, $^2J_{CP} = 17.2$–14.1 Hz). Strong IR ν_{CN} bands were also apparent (2123–2142 cm^{-1}).

All of the complexes in Scheme 4 showed only a single set of *n*/2 methylene ^{13}C NMR signals. In this context, consider the idealized conformational energy minimum **VI** in Scheme 5, which features a mirror plane. This would give rise to two sets of *n*/2 methylene ^{13}C NMR signals with a 2:1 intensity ratio. Thus, ^1H and $^{13}C\{^1H\}$ NMR spectra of *trans*-**4c**, *trans*-**5c**, *trans*-**10c**, and *trans*-**12c** were recorded in $CDFCl_2$[24] at low temperatures. However, even at $-120\,^\circ C$, no decoalescence—only signal broadening—was observed. Hence, the MCl_2, MBr_2, MI_2, and $M(CN)_2$ moieties appear to have very low rotational barriers, rendering the three methylene bridges equivalent on the NMR timescale. The carbon–phosphorus coupling seen in the cyanide ligand ^{13}C NMR signals rules out alternative dynamic processes involving dissociation of the cyanide or diphosphine ligands.

Complexes with more longitudinally extended rotors were sought. Thus, *trans*-**4c** and the thiocyanide salt KSCN (4.1 equiv) were combined in THF/acetone (homogeneous conditions). As shown in Scheme 6 (top), a chromatographic workup gave two white crystalline products, *trans*-**13c** and

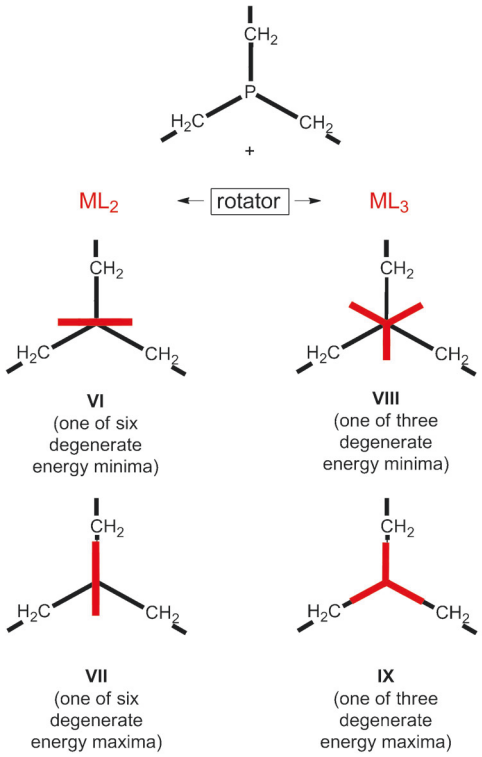

Scheme 5. Effect of rotator symmetry upon numbers and types of energy minima and maxima in gyroscope-like complexes.

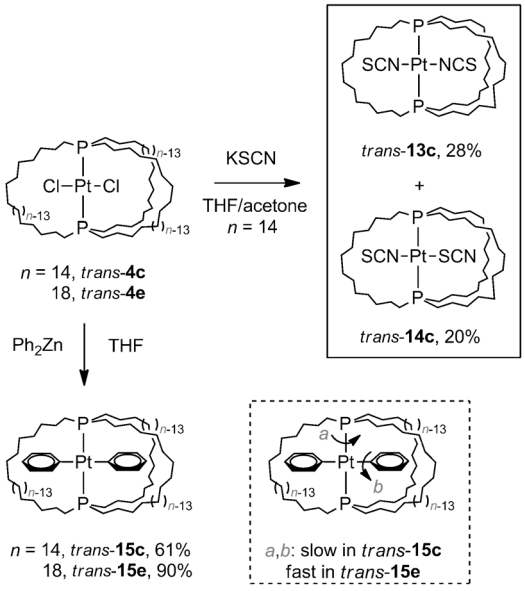

Scheme 6. Additional chloride ligand substitution reactions.

trans-**14c**, in 28 and 20% yields, respectively. When a similar reaction was monitored by ^{31}P NMR spectroscopy, the initial **13c**/**14c** ratio was about 50:50, and shifted with time in favor of *trans*-**14c**.[25]

Complex *trans*-**13c** exhibited a single IR ν_{NCS} band (2111 cm^{-1}), and a crystal structure (below) showed two nitrogen bound or isothiocyanide ligands. Complex *trans*-**14c** exhibited two IR ν_{NCS} bands, one close to that of *trans*-**13c** (2107 cm^{-1}), and the other at a lower frequency (2005 cm^{-1})—a shift typical of a thiocyanide ligand.[26] Hence, *trans*-**14c** was assigned as an unsymmetrical NCS/SCN linkage isomer.[27] In a series of palladium thiocyanide/isothiocyanide adducts with diphosphine ligands $Ph_2P(CH_2)_{m'}PPh_2$ ($m'=2$, 3, 4), either the SCN/SCN, NCS/SCN, or NCS/NCS isomers can dominate, depending upon chelate ring size.[28] Importantly, the ^{13}C NMR spectra of *trans*-**13c** and *trans*-**14c** exhibited 12 and 13 methylene carbon signals, respectively, showing PtX_2 rotation to be slow on the NMR timescale at room temperature.[29]

Finally, *trans*-**4c**,**e** were combined with the carbon nucleophile Ph_2Zn (3.0 equiv) in THF. After 20 h, NMR spectra showed that substitution was $\geq$95% complete. As depicted in Scheme 6 (bottom), workups gave the corresponding diphenyl complexes *trans*-**15c** and *trans*-**15e** as white air stable powders in 61–90% yields. The ^{13}C NMR spectrum of *trans*-**15c** showed 14 methylene carbon signals, or two sets of seven (n/2) with an approximate 2:1 intensity ratio. However, that of *trans*-**15e** showed only nine signals. This indicates slow and fast $PtPh_2$ rotation, respectively, on the NMR timescale at room temperature. Interestingly, the ^1H and ^{13}C NMR spectra of *trans*-**15c** exhibited two *ortho*- and two *meta*-phenyl CH signals. This further requires restricted rotation about the Pt–C_{ipso} axis as depicted in Scheme 6. No coalescence or line broadening was observed when spectra were recorded at 80 °C in $CDCl_3$. The ^1H and ^{13}C NMR spectra of *trans*-**15e** did not exhibit additional phenyl signals at room temperature.

Crystal structures of gyroscope-like complexes

As noted above, single crystals of many complexes could be obtained. The crystal structures of six platinum and palladium dichloride, dibromide, and diiodide complexes with 14 carbon methylene segments, *trans*-**4c**, *trans*-**7c**, *trans*-**9c**, *trans*-**5c**, *trans*-**8c**, and *trans*-**10c**, were determined as summarized in the Experimental Section and Table S1 in the Supporting Information. With *trans*-**5c** and *trans*-**7c**, four to five carbon atoms were disordered, but the major and minor conformations could be resolved. Unit cell parameters and selected interatomic distances and bond angles are provided in Table 2. Views of each structure are given in Figures 1–6.

The crystal structures of two additional platinum complexes with 14 carbon methylene segments were determined, the bis(isothiocyanide) complex *trans*-**13c** and a pentane monosolvate of the diphenyl complex, *trans*-**15c**·*n*-C_5H_{12}. With the former, which exhibited a C_2 axis perpendicular to the coordination plane, four carbon atoms were disordered and refined with 50:50 occupancy ratios. The N–Pt–N and N=C=S linkages were nearly linear (178.8(2)° and 178.6(5)°), but consistent with literature structures[28] the Pt–N=C linkage was more bent (169.6(5)°). The crystal structure of the diphenyl complex with 18 carbon methylene segments, *trans*-**15e**, could also be determined. Data for these compounds are incorporated into Table 2, and the molecular structures are depicted in Figures 7–9.

Table 2. Lattice parameters and key interatomic distances [Å] and angles [°] for gyroscope-like complexes.

	trans-**4c**	*trans*-**7c**	*trans*-**9c**	*trans*-**5c**	*trans*-**8c**	*trans*-**10c**	*trans*-**13c**	*trans*-**15c** ·*n*-C_5H_{12}	*trans*-**15e**
space group	$P2_1/n$	$P2_1/n$	*Pbca*	$P2_1/n$	$P2_1/n$	*Pbca*	*C*2/*c*	$P\bar{1}$	$P\bar{1}$
a [Å]	16.264(3)	16.2375(4)	20.702(4)	16.2233(2)	16.318(7)	20.737(4)	18.225(4)	11.9863(2)	9.4061(2)
b [Å]	13.698(3)	13.9462(4)	13.778(3)	13.7836(3)	13.796(6)	13.785(3)	15.265(4)	16.4670(3)	13.1694(2)
c [Å]	19.998(4)	20.2226(5)	33.197(6)	20.1744(4)	20.043(9)	33.259(5)	18.179(4)	16.9113(2)	28.3030(5)
α [°]	90	90	90	90	90	90	90	67.387(1)	79.746(1)
β [°]	91.29(3)	90.31(3)	90	91.207(1)	90.52(4)	90	104.27(3)	72.547(1)	80.949(1)
γ [°]	90	90	90	90	90	90	90	79.382(1)	71.449(1)
V [Å^3]	4454.1(16)	4579.4(2)	9469(3)	4510.31(14)	4512(3)	9507(3)	4901(2)	2930.44(8)	3251.61(10)
Z	4	4	8	4	4	8	4	2	2
M–P1	2.3051(8)	2.3100(13)	2.3207(17)	2.3199 (6)	2.317(4)	2.3398(9)	2.3189(15)	2.2849(7)	2.2838(11)
M–P2	2.3082(8)	2.3169(13)	2.3278(17)	2.3129(6)	2.319(4)	2.3470(9)	2.3189(15)	2.2845(7)	2.2761(11)
M–X1	2.3165(10)	2.4281(8)	2.6192(6)	2.2976(6)	2.416(2)	2.6183(5)	1.961(4)	2.079(3)	2.096(4)
M–X2	2.3074(10)	2.4313(8)	2.6045(7)	2.3080(6)	2.384(2)	2.5988(5)	1.961(4)	2.080(3)	2.092(4)
P1···P2	4.611	4.625	4.646	4.630	4.633	4.685	4.634	4.568	4.559
X-M-X	178.10(3)	177.13(2)	173.508(18)	177.49(3)	176.98(9)	172.891(11)	178.8(2)	175.87(10)	179.13(16)
P-M-P	176.75(3)	177.10(5)	176.64(6)	176.15(2)	175.74(14)	176.55(3)	175.00(6)	176.74(2)	177.74(4)

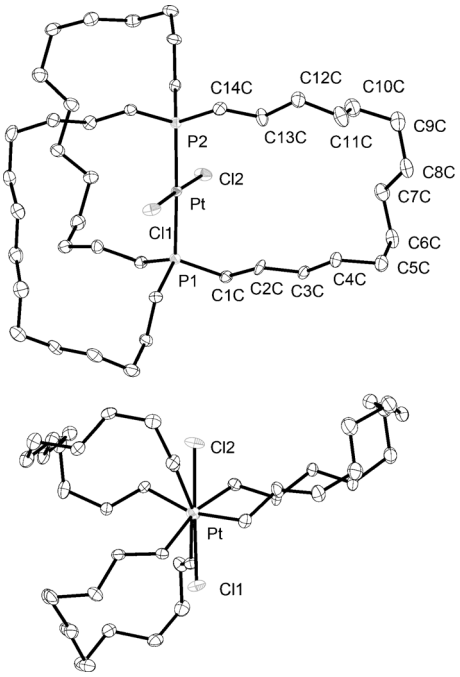

Figure 1. Thermal ellipsoid plots of *trans*-**4c** (50% probability level): side view (top); view along P2-Pt-P1 axis (bottom).

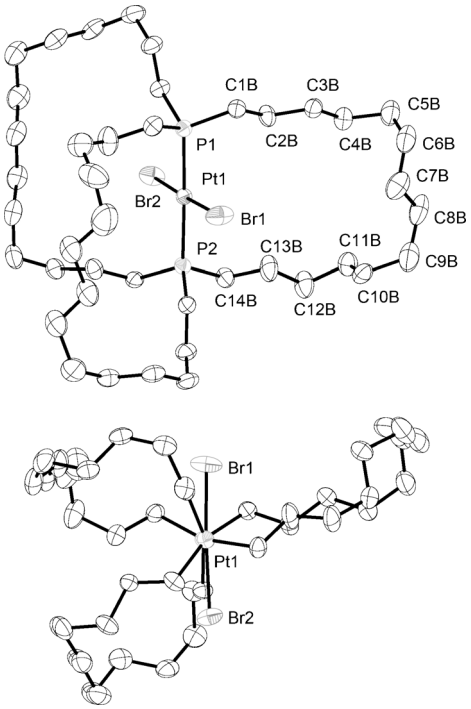

Figure 2. Thermal ellipsoid plots of *trans*-**7c** (50% probability level): side view (top); view along P2-Pt-P1 axis (bottom). Five carbon atoms are disordered; the dominant conformation is depicted.

Other metrical parameters, of interest in the context of analyses presented in the discussion section, were also tabulated. Torsion angles associated with the methylene segments are presented in Tables 3 and 4 in a format that facilitates identification of "conserved conformations". Table 5 provides other quantities associated with individual molecules or the crystal lattice.

Demetalation reactions

In the course of exploring the above substitution chemistry, unexpected demetalations that liberated the diphosphine ligands were discovered. Although these represent the start of major ongoing investigations involving the demetalation mechanism and diphosphine properties,[30,31] certain results bear upon key synthetic or structural issues above. Hence, selected observations are presented here.

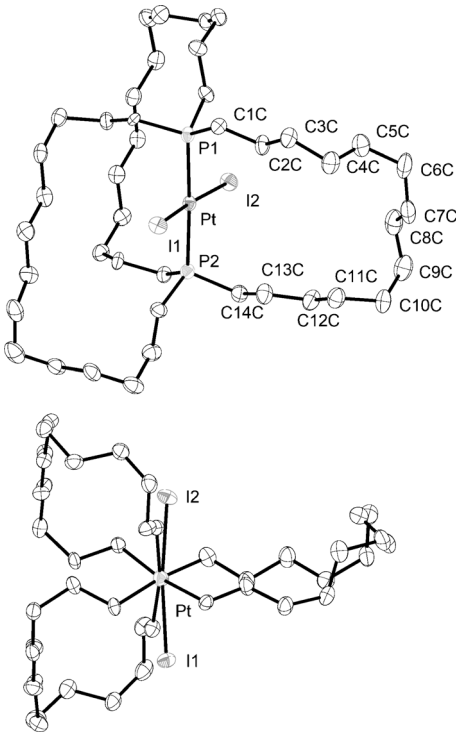

Figure 3. Thermal ellipsoid plots of *trans*-**9c** (50% probability level): side view (top); view along P2-Pt-P1 axis (bottom).

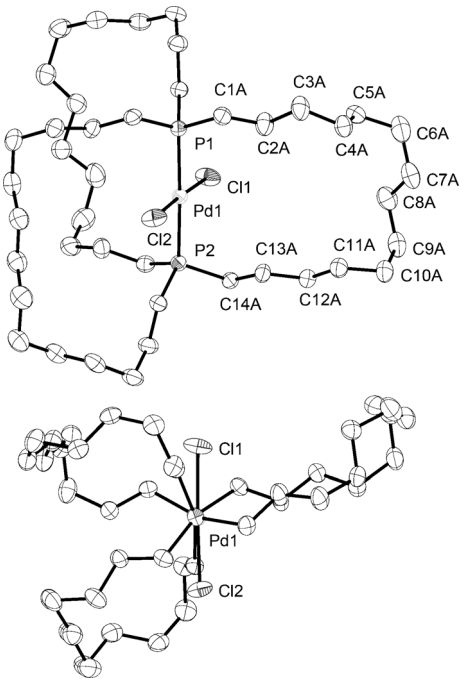

Figure 4. Thermal ellipsoid plots of *trans*-**5c** (50% probability level): side view (top); view along P2-Pd-P1 axis (bottom). Four carbon atoms are disordered; the dominant conformation is depicted.

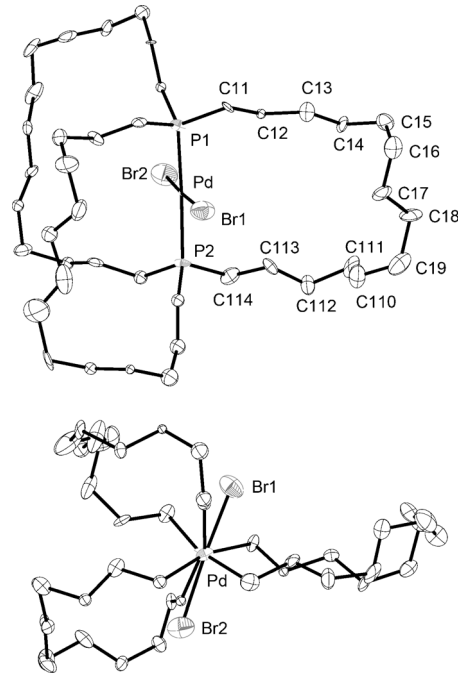

Figure 5. Thermal ellipsoid plots of *trans*-**8c** (50% probability level): side view (top); view along P-Pd-P axis (bottom).

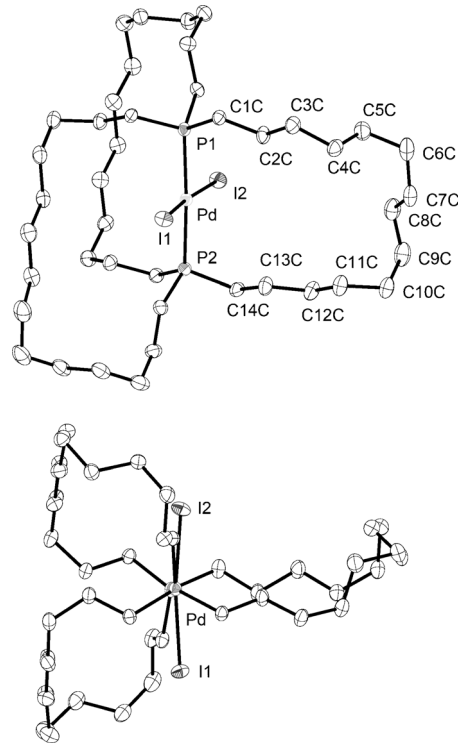

Figure 6. Thermal ellipsoid plots of *trans*-**10c** (50% probability level): side view (top); view along P2-Pd-P1 axis (bottom).

Small-scale reactions of *trans*-**4c** and NaC≡CH (2–4 equiv; commercial xylene slurry or powder) in THF were monitored by ^{31}P NMR spectroscopy. The reactants were gradually consumed over the course of 24–48 h. As shown in Scheme 7, the data suggested the formation of both mono- (*trans*-**16c**; 9.83 ppm, $^{1}J_{PPt} = 2429$ Hz) and disubstituted (*trans*-**17c**; 6.46 ppm, $^{1}J_{PPt} = 2421$ Hz) products. In an effort to promote complete conversion to *trans*-**17c**, a larger excess of NaC≡CH (30 equiv) was employed. However, now a third species, with

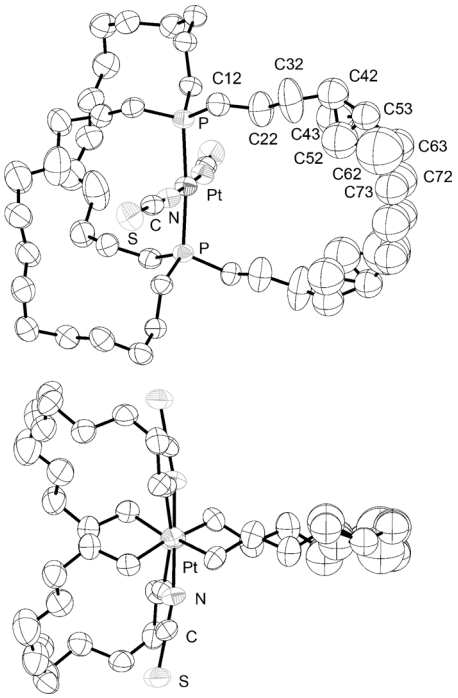

Figure 7. Molecular structure of *trans*-**13 c** with atoms represented as isotropic spheres: side view (top); view along P-Pt-P axis (bottom).

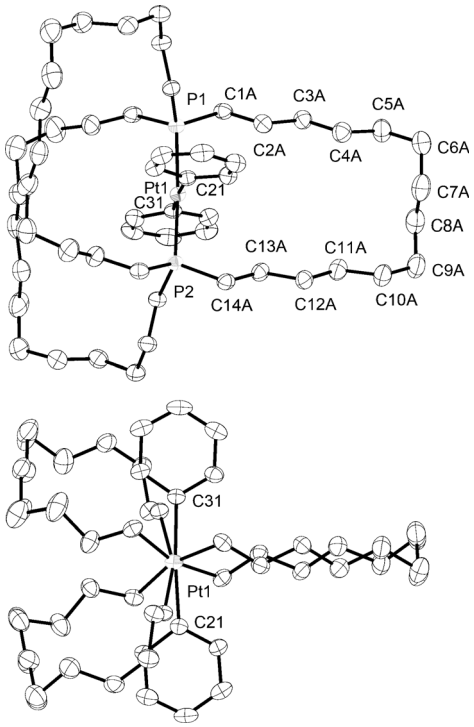

Figure 8. Thermal ellipsoid plots of *trans*-**15 c**·*n*-C_5H_{12} with solvent molecule omitted: side view (top); view along P2-Pt-P1 axis (bottom).

a signal that was not coupled to platinum, was clearly observed (**18**, −31.9 ppm). After 140 h, *trans*-**16 c** and *trans*-**17 c** could no longer be detected. Workup of a comparable preparative reaction gave **18** as a moderately air-sensitive white powder in 91% yield. Based upon the mass spectrum, microanalysis, and chemistry described elsewhere,[30,31] this was assigned as the dibridgehead diphosphine corresponding to the stator of *trans*-**4 c**.

The isomeric complex *trans*-**4′c** and NaC≡CH (5–50 equiv) were also combined in THF at room temperature. After 9 d, workup gave the isomeric diphosphine $(\overbrace{CH_2)_{14}P(CH_2)_{14}P(CH_2)_{14}}$ (**19**) as a white powder in 90% yield. Alternatively, the crude

Table 3. Torsion angles [°] for gyroscope-like complexes with $P(CH_2)_{14}P$ linkages for *trans*-**4 c**, *trans*-**7 c**, *trans*-**9 c**, and *trans*-**5 c**.[a]

	trans-**4 c**	*trans*-**7 c**	*trans*-**9 c**	*trans*-**5 c**
P1-C1-C2-C3	178.2(2)/177.8(2)/−167.0(2)	−168.8(4)/173.8(5)/177.8(4)	168.0(5)/174.2(5)/179.4(5)	172.4(2)/−176.44(17)/167.42(18)
C1-C2-C3-C4	−55.9(4)/54.7(4)/176.3(3)	175.6(5)/−63.8(8)/54.0(7)	−63.2(7)/56.3(8)/170.3(6)	163.8(3), −155.9(6)[b]/55.9(3)/−178.8(2)
C2-C3-C4-C5	−53.8(4)/60.9(4)/−179.0(3)	−178.3(5)/−49.5(10)/59.4(7)	−61.8(8)/62.4(8)/71.6(8)	61.7(4),−69.7(10)[b]/57.5(3)/61.3(3)
C3-C4-C5-C6	−58.5(4)/178.1(3)/56.2(4)	58.3(7)/−77.4(12),−57.8(12)[b]/179.0(5)	−179.5(6)/178.2(6)/174.6(7)	174.7(2),−176.8(7)[b]/−178.8(2)/60.3(3)
C4-C5-C6-C7	−174.0(3)/71.2(4)/55.9(4)	53.6(8)/−176.2(9),180(11)[b]/71.6(7)	179.3(6)/60.8(8)/63.1(10)	66.8(4),171.4(9)[b]/92.0(3),51.7(7)[b]/179.6(2)
C5-C6-C7-C8	178.1(3)/72.1(4)/63.9(4)	63.9(7)/−170.7(12),62(2)[b]/72.4(7)	172.6(6)/58.6(8)/60.8(10)	61.6(4),79.2(6)[b]/−66.7(4), 72.0(12)[b]/−177.1(2)
C6-C7-C8-C9	−176.9(3)/178.7(3)/177.4(3)	−179.6(5)/−172.1(10),174.8(11)[b]/177.8(5)	174.8(6)/173.9(6)/172.0(6)	179.2(2)/−178.5(3),173.5(8)[b]/178.8(2)
C7-C8-C9-C10	−64.7(4)/−176.1(3)/62.5(4)	61.2(9),78.5(11)[b]/−67.2(12), 66.9(12)[b]/−177.4(5)	56.8(9)/176.4(6)/60.1(9)	64.6(3)/178.2(3), 77.4(13)[b]/72.4(3)
C8-C9-C10-C11	91.7(3)/−179.6(3)/67.0(4)	68.6(9),168.5(15)[b]/93.6(7), 51.6(9)[b]/−179.4(5)	63.0(8)/−177.3(6)/53.6(10)	54.3(3)/−172.2(3),159.1(8)[b]/71.3(3)
C9-C10-C11-C12	−179.2(2)/60.0(4)/174.8(3)	173.3(6),−175.5(13)[b]/−179.1(5)/61.6(7)	−178.8(6)/−179.7(6)/59.9(9)	57.7(3)/−59.7(4)/178.3(2)
C10-C11-C12-C13	57.0(4)/59.8(4)/60.9(4)	−67.7(17),61.3(9)[b]/57.9(6)/63.3(7)	63.8(8)/−62.9(8)/−176.4(7)	−178.5(2)/−52.9(4)/60.3(3)
C11-C12-C13-C14	55.1(4)/−178.8(3)/165.1(3)	161.8(6),−157.7(9)[b]/56.1(6)/−177.8(5)	56.6(8)/−62.8(8)/176.9(6)	175.4(2)/−58.5(3)/55.7(3)
C12-C13-C14-P2	−175.9(2)/168.0(2)/172.2(2)	171.5(5)/−177.1(4)/164.0(4)	171.4(5)/165.5(5)/−163.1(5)	−167.94(17)/178.57(18)/178.27(18)

[a] The torsion angles for each of the three $P(CH_2)_{14}P$ segments are separated by slashes. [b] One or more carbon atoms associated with this torsion angle are disordered. The first value represents that derived from the carbon atoms with the greater occupancy factors (dominant conformation). The second value represents that from the carbon atoms with the lower occupancy factors.

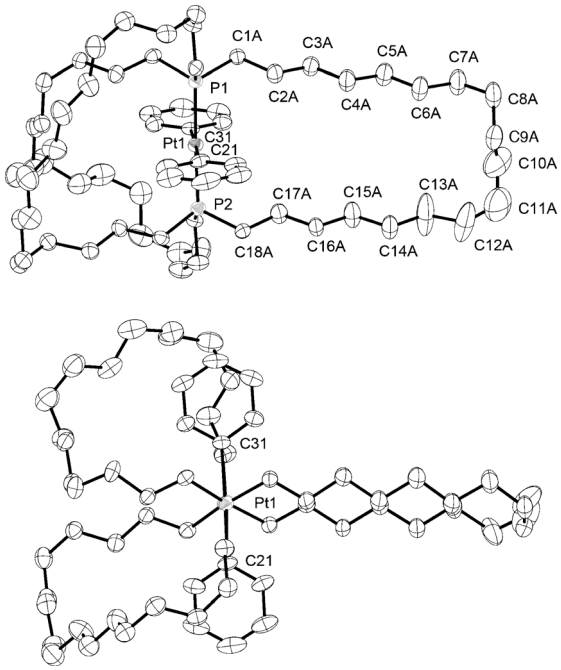

Figure 9. Thermal ellipsoid plots of *trans*-**15e**: side view (top); view along P2-Pt-P1 axis (bottom).

product was treated with $BH_3{\cdot}S(CH_3)_2$. This gave the previously reported[30] bis(borane) adduct **19**·$(BH_3)_2$ as a white solid in 78% overall yield. Single crystals were obtained, and the crystal structure determined (Experimental Section). The molecular structure and key metrical parameters are given in Figure 10. This unequivocally establishes the nature of the ligand in *trans*-**4′c** and related complexes above.

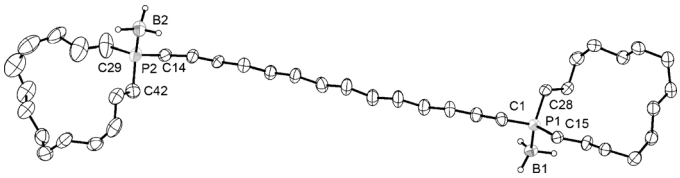

Figure 10. Thermal ellipsoid plot of **19**·$2BH_3$ (50% probability level). Key crystallographic distances (Å) and bond angles (°): P1···P2 19.406(9), P1—B1 1.903(5), P2—B2 1.916(5), P1—C1 1.823(4), P1—C15 1.811(4), P1—C28 1.806(4), P2—C14 1.797(5), P2—C29 1.848(6), P2—C42 1.802(5), C1-P1-B1 113.4(2), C15-P1-B1 113.4(2), C28-P1-B1 114.6(2), C14-P2-B2 113.8(2), C29-P2-B2 111.4(3), C42-P2-B2 113.9(3), C1-P1-C15 102.4(2), C15-P1-C28 107.3(2), C28-P1-C1 104.7(2), C14-P2-C29 103.5(2), C29-P2-C42 110.1(3), C42-P2-C14 103.4(2).

Discussion

Scope of syntheses

Scheme 2 shows that dichloroplatinum- and dichloropalladium-based gyroscope-like complexes can be accessed in fair to low overall yields by means of ring-closing metathesis/hydrogenation sequences involving *trans*-phosphine ligands of the formula $P((CH_2)_mCH{=}CH_2)_3$, in which *m* is greater than or equal to six. Systems with 17-membered macrocycles (*trans*-**4c**, *trans*-**5c**) and 14 methylene groups are most efficiently obtained, and appreciable quantities of 21-membered analogues can also be isolated.

Reactions with dibromo analogues (Scheme 3) are slower, and give byproducts arising from catalyst-derived chloride/bromide exchange. Exchange was not a problem in a similar sequence involving an octahedral rhenium bromide complex.[10] However, PtO_2 was used as the hydrogenation catalyst, and the yield was lower than with the rhenium chloride analogue. These data suggest that smaller ligands are advantageous for threefold interligand alkene metathesis. Indeed, when one of the chloride ligands in *trans*-**1c** is replaced by a pentafluorophenyl ligand, only oligomers are obtained.[32]

Ring-closing metatheses of pentafluorophenyl-substituted platinum chloride complexes with *trans*-diphenylphosphine ligands of the formula $Ph_2P(CH_2)_mCH{=}CH_2$ have also been investigated.[33] In these cases, metathesis/hydrogenation sequences efficiently yield 13 to 23-membered macrocycles with 10–20 methylene groups (*m* = 4, 67%; 5, 82%; 6, 69%; 8, 53%; 9, 43%). The failure to detect monometallic products from the substrates with *m* = 4 and 5 in Scheme 2 may in part reflect

Table 4. Torsion angles [°] for gyroscope-like complexes with $P(CH_2)_{14}P$ linkages for *trans*-**8c**, *trans*-**10c**, *trans*-**13c**, and *trans*-**15c**·*n*-C_5H_{12}.[a]

	trans-**8c**	*trans*-**10c**	*trans*-**13c**	*trans*-**15c**·*n*-C_5H_{12}
P1-C1-C2-C3	−162.7(8)/−180.0(10)/172.9(9)	167.4(2)/174.0(2)/179.6(2)	175.3(4)/−176.2(8)/157.9(5)	−161.7(3)/−177.4(2)/169.4(2)
C1-C2-C3-C4	173.1(11)/−61.6(17)/55.1(16)	−64.0(4)/56.3(4)/171.0(3)	56.4(7)/−164.1(13)/−76.6(8)	168.1(4)/−58.1(4)/−179.9(3)
C2-C3-C4-C5	179.3(11)/−52(2)/56.3(17)	−62.9(4)/62.2(4)/71.2(4)	58.9(7)/−88.4(19)/−172.9(9)	−69.8(5)/−65.9(4)/177.3(3)
C3-C4-C5-C6	56.9(18)/−58(2)/174.7(12)	−179.6(3)/177.9(3)/173.7(3)	171.2(5)/−143(3)/−169.8(9)	−80.2(5)/−175.4(3)/180.0(3)
C4-C5-C6-C7	52.4(19)/−174.9(14)/73.4(17)	179.5(3)/61.7(4)/63.9(5)	63.8(8)/−129(2)/−70.5(12)	178.3(3)/−64.7(4)/59.8(5)
C5-C6-C7-C8	68.9(17)/174.9(16)/68.6(17)	172.5(3)/58.8(4)/60.9(5)	61.2(9)/−96(3)[b]/−174.8(7)	−179.5(3)/−62.9(5)/58.6(5)
C6-C7-C8-C9	176.8(12)/−178.1(15)/−177.6(11)	174.8(3)/174.2(3)/170.4(3)	172.4(6)/146(3)[b]/172.4(6)	−173.0(3)/−176.5(3)/178.2(3)
C7-C8-C9-C10	63.3(18)/−57(2)/−171.5(11)	56.2(4)/176.4(3)/58.9(4)	−174.8(7)/−96(3)[b]/61.2(9)	−56.7(5)/−179.3(3)/59.6(4)
C8-C9-C10-C11	66(2)/90.3(16)/−177.7(11)	64.4(4)/−177.8(3)/54.1(4)	−70.5(12)/−129(2)[b]/63.8(8)	−64.1(5)/177.8(3)/59.9(4)
C9-C10-C11-C12	174.1(14)/−179.5(12)/57.8(15)	−179.1(3)/−180.0(3)/60.0(4)	−169.8(9)/−143(3)[b]/171.2(5)	−175.2(3)/−71.8(4)/178.6(3)
C10-C11-C12-C13	62.7(17)/52.6(16)/63.5(15)	63.5(4)/−62.1(4)/−176.8(3)	−172.9(9)/−88.4(19)[b]/58.9(7)	−65.5(4)/−70.4(4)/177.7(3)
C11-C12-C13-C14	161.7(12)/57.6(16)/178.4(10)	56.4(4)/−65.2(4)/177.6(3)	−76.6(8)/−164.1(13)[b]/56.4(7)	−59.1(4)/172.9(3)/−179.4(3)
C12-C13-C14-P2	169.3(10)/−175.5(9)/162.7(9)	170.7(2)/167.2(2)/−163.6(2)	157.9(5)/−176.2(18)[b]/175.3(4)	−175.9(2)/−162.3(2)/169.6(2)

[a] The torsion angles for each of the three $P(CH_2)_{14}P$ segments are separated by slashes. [b] One or more carbon atoms associated with this torsion angle are disordered with 50:50 occupancy factors. The torsion angle given is for the chain with the better geometrical parameters.

Table 5. Intramolecular and intermolecular distances involving rotator and stator atoms in gyroscope-like complexes [Å], and angles defined by gyroscope axes [°].

	trans-**4c**	*trans*-**7c**	*trans*-**9c**	*trans*-**5c**	*trans*-**8c**	*trans*-**10c**	*trans*-**13c**	*trans*-**15c** ·*n*-C_5H_{12}	*trans*-**15e**
M–X[a]	2.312	2.430	2.612	2.303	2.400	2.609	4.708[b]	5.883[c]	5.873[c]
radius of rotator[d]	4.062	4.280	4.592	4.053	4.250	4.589	6.508	7.083	7.073
M–C_a[e]	7.448	7.448	7.295[f]	7.438	7.453	7.293	7.38[g]	7.790	10.373
M–C'_a[e]	6.746	6.798	6.589	6.762	6.736	6.529	7.38[g]	7.760	10.486
M–C_b[e]	6.385	6.461[h]	5.630	5.741	5.691	6.682	6.954	5.774	5.915
M–C'_b[e]	5.734	5.566[h]	5.490	6.383	6.441	5.635	6.001	5.206	6.162
M–C_c[e]	5.457	6.388	5.629	6.394[h]	6.342	5.642	6.001	5.348	7.928
M–C'_c[e]	6.350	5.735	6.676	5.518[h]	5.434	6.713	6.954	5.759	7.793
M–$C_{distal\text{-}vdW}$[i]	3.757	3.866	3.790	3.818	3.734	3.935	4.301	3.506	4.215
M–$C_{distal'\text{-}vdW}$[j]	5.748	5.748	5.595	5.738	5.753	5.593	5.68[g]	6.090	8.786
M–$C_{neighbor}$[k]	4.619	4.800	5.878	4.685	4.714	5.869	5.020(8)	6.153	5.732
M–$C_{neighbor\text{-}vdW}$[l]	2.919	3.100	4.178	2.985	3.014	4.169	3.320(8)	4.453	4.032
∢ [P-M-P + P-M-P][m]	79.42	78.07	[n]	79.16	79.87	[n]	[o]	[o]	[o]
∢ [P-MX_2-P][m]	79.74	78.14	[n]	79.00	78.84	[n]	[o]	[o]	[o]

[a] The crystallographic distances (Table 2) are averaged. [b] Distance from platinum to the non-bonded sulfur atom. [c] Distance from platinum to the *para*-hydrogen atom of the phenyl ring. [d] M–X plus the van der Waals radius of the terminal atom (halide, sulfur, or hydrogen). [e] Distance from the metal to the two remote carbon atoms of the macrocycles that are closest to the plane of the rotator (M–C_{distal}). The indices a, b, and c refer to the three different macrocycles as illustrated in Figure 11. [f] In this complex, a carbon atom adjacent to this atom was the farthest from the metal (7.388 Å). [g] These distal carbon atoms are disordered with a 50:50 occupancy ratio. The average distance to the metal is given. [h] These distal carbon atoms are disordered with 53:47 or 82:18 occupancy ratios. The distance corresponds to that to the remote carbon with the greater occupancy factor. [i] The shortest of the previous six distances, minus the van der Waals radius of carbon (1.70 Å). [j] The longest of the previous six distances, minus the van der Waals radius of carbon. [k] Distance from the metal to the nearest carbon atom of a neighboring molecule. [l] Previous entry minus the van der Waals radius of carbon. [m] Planes used for angle calculations between sets of molecules with parallel P-M-P axes; see also the text and Figure 14. [n] This lattice exhibits four sets of molecules with parallel P-M-P axes. [o] All of the P-M-P axes in the lattice are parallel.

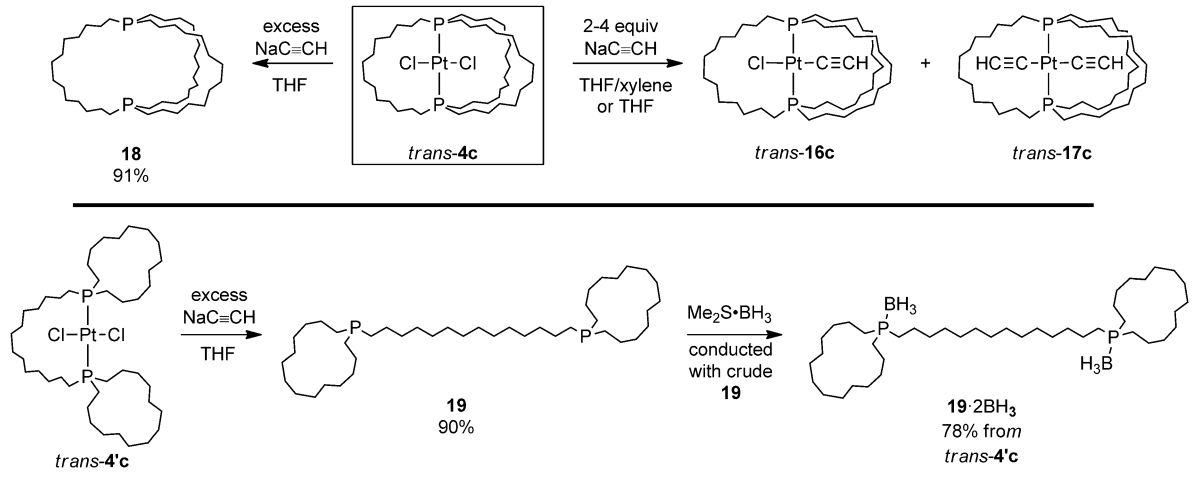

Scheme 7. Isolations of diphosphines by demetalations of platinum complexes.

a greater likelihood for intermolecular metathesis with multiple shorter chain $(CH_2)_mCH{=}CH_2$ substituents.

In this context, it should be noted that the trigonal bipyramidal iron tricarbonyl analogs **III** (Scheme 1) can be accessed in good overall yields from precursors *trans*-$Fe(CO)_3(P((CH_2)_mCH{=}CH_2)_3)_2$ with $m = 4$ (50–64%), 5 (63%), 6 (64%), and 8 (74%).[6] The superior yields may in part be due to a preorganization effect. Specifically, both the $Fe(CO)_3$ fragment and phosphine ligands have a C_3 symmetry axis. In the precursors, each phosphine ligand would logically adopt a conformation in which the $(CH_2)_mCH{=}CH_2$ substituents are staggered with respect to the CO ligands, as shown in **X** in Scheme 8. This directs the $(CH_2)_mCH{=}CH_2$ groups that must metathesize to afford **III** into the same interstices. Once one linkage is in place, subsequent intramolecular and interligand metathesis becomes more probable.

In contrast, consider the limiting conformations **XI** and **XII** depicted in Scheme 8 for the dichloroplatinum and dichloropalladium precursors. The latter directs three phosphine substituents on each side of the metal square plane, while minimizing P-M-P torsional interactions, and may be the more stable. In any case, after an initial interligand macrocyclization

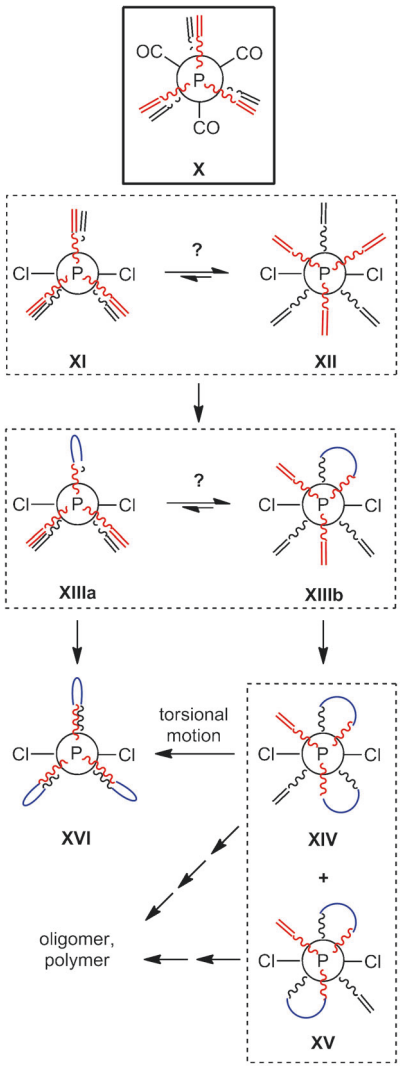

Scheme 8. Some conformational considerations in ring-closing metatheses leading to gyroscope-like complexes.

of **XI** or **XII**, an equilibrium mixture of conformers **XIII a** and **XIII b** should result. While the former is positioned to lead to the gyroscope-like product **XVI**, the latter can undergo either 1) a productive macrocyclization to give **XIV**, which can with appropriate torsional motion be transformed to **XVI**, or 2) a dead-end macrocyclization to give **XV**, which due to mismatched connectivity can only lead to oligomer or polymer. The latter has no counterpart in a trigonal-bipyramidal geometry.

Except in the case of *trans*-**1 e**, the yields of products derived from a combination of inter- and intraligand metathesis (*trans*-**4′c,d,e**, *trans*-**5′e**; Scheme 2) are much lower than those of the gyroscope-like complexes. They may be derived from **XIII** in Scheme 8, or by initial intraligand metathesis. Analogous products have not yet been detected with any trigonal-bipyramidal substrate. However, they can be observed with various octahedral substrates,[34] and one has been crystallographically characterized. No attempt has been made to establish thermodynamic control in any of these reactions, although this has been unambiguously attained in other cases.[35] Also, there remain possibilities for optimizing the preceding chemistry. For example, Fogg has emphasized that oligomers sometimes dominate kinetically in ring-closing metatheses, but can convert to monocyclic products given sufficient time, catalyst, and ethylene co-product.[36]

Some conceptually related synthetic efforts from other research groups merit note. Setaka and co-workers have shown that threefold intramolecular olefin metatheses can be effected with several aromatic systems that bear *para*-substituents of the formula $Si((CH_2)_mCH{=}CH_2)_3$.[16c,e] A representative sequence leading to the gyroscope-like bis(silane) **21**, which features a *p*-phenylene rotator and 20-membered macrocycles, is shown in Scheme 9 (top). Related compounds with silicon containing spokes have been accessed by other routes.[16a,b]

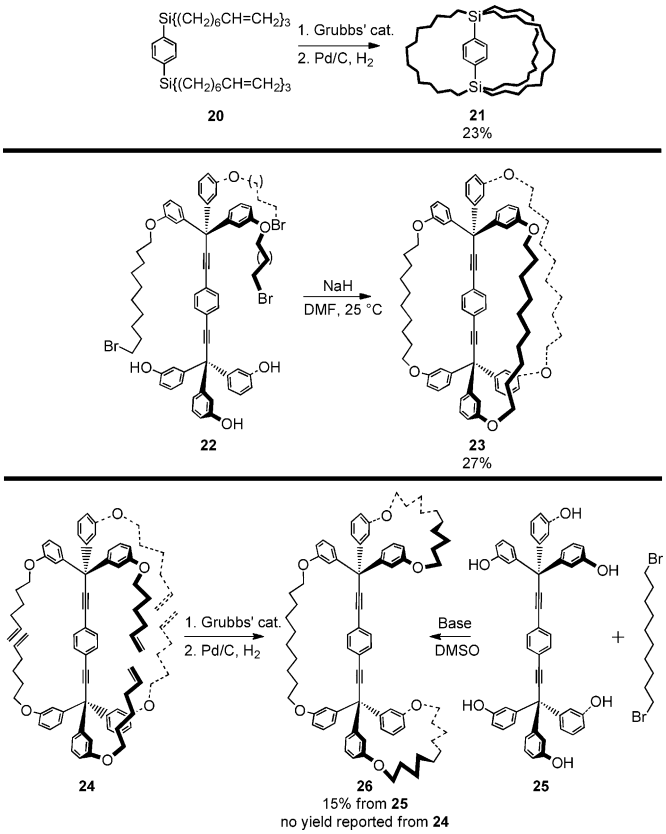

Scheme 9. Gyroscope-like organic and organosilicon molecules and related species synthesized by the Garcia-Garibay and Setaka groups.

The Garcia-Garibay group has reported that the gyroscope-like molecule **23**, which features 28-membered macrocycles, can be obtained in 27% yield by a threefold intramolecular Williamson ether synthesis using the tris(phenol) **22** (Scheme 9, middle).[15a,b] Interestingly, reaction of the hexa(alkene) **24** with Grubbs' catalyst afforded only the isomer **26** after hydrogenation, which is derived from a combination of inter- and intra-endgroup metathesis. This is opposite to the dominant cyclization mode found with all coordination geometries in Scheme 1. Homologues with shorter and longer methylene

chains gave analogous results. An intermolecular Williamson ether synthesis with the hexa(phenol) **25** and an α,ω-dibromide also afforded **26** (Scheme 9, bottom). However, reactions of **25** with other types of α,ω-electrophiles gave low yields of compounds with topologies analogous to **23**.[15b]

Structural data: bond lengths, bond angles, and torsion angles

Several platinum and palladium dichloride, dibromide, and diiodide complexes of the formula *trans*-[$MX_2(PR_3)_2$] have been crystallographically characterized.[37] The six new dihalide complexes presented above (Figure 1–Figure 6) are unexceptional from the standpoint of bond lengths about the metals. As summarized in Table 2, the X-M-X angles in the diiodide complexes *trans*-**9c** and *trans*-**10c** exhibit the greatest deviations from 180° (172.891(11) and 173.508(18)°), perhaps reflecting repulsive interactions of this larger ligand with the macrocycles; values of $>179.5°$ are common in acyclic analogues.[37d,f] The smallest P-M-P angle is found in the palladium dibromide complex *trans*-**8c** (175.74(14)°). Among the three non-halide complexes, the X-M-X and P-M-P angles in the diphenyl adduct *trans*-**15c** are the smallest (175.87(10) and 176.74(2)°).

The torsion angle data in Table 3 reveal a number of relationships for the eight complexes with $P(CH_2)_{14}P$ linkages. In all adducts, the terminal P1-C1-C2-C3 and C12-C13-C14-P2 segments adopt *anti* conformations, with torsion angles ranging from $\pm157.9(5)$ to $\pm180.0(10)°$. Similarly, the middle C6-C7-C8-C9 segments are also *anti*, with torsion angles ranging from $\pm179.6(5)$ to $\pm170.4(3)$ or $\pm146(3)°$ (disordered chain). These units can be viewed as the "top", "bottom", and "sides" of the stators, and crystallize as linearly as possible. The intermediate segments feature a mixture of *anti* and *gauche* conformations, with the latter providing the necessary "curvature".

Of the 24 macrocycles in these eight complexes, 17 exhibit seven *anti*-$PCH_2CH_2CH_2$ or -$CH_2CH_2CH_2CH_2$ segments and six *gauche* segments (totals reflect the dominant conformations of the three disordered chains). Four possess six *anti* and seven *gauche* segments, and one has eight and five. Both *trans*-**13c** and *trans*-**15c** exhibit one macrocycle with nine *anti* and four *gauche* segments, and the distinctive motif in the latter is analyzed in the following paragraph. The most striking homology involves the platinum and palladium diiodide complexes *trans*-**9c** and *trans*-**10c**, for which all rings exhibit identical *anti*/*gauche* sequences (seven and six total), and nearly identical torsion angles. Less extended homologous sequences in the other complexes are readily apparent in Figure 1–Figure 8.

The diphenyl complex *trans*-**15e** (Figure 9) features 21-membered macrocycles with 18 methylene groups, each of different conformational types. Interestingly, *trans*-**15e** and the lower homologue *trans*-**15c** (Figure 8) both have one ring with two extended series of *anti* segments (P1 to C6A or C8A and C9A or C11A to P2), connected by a "curved" *gauche*/*gauche*/*anti*/*gauche*/*gauche* sequence. This motif is not found in any of the other complexes. The conformation about the phosphorus–phosphorus vector (CH_2—P···P—CH_2) in *trans*-**15e** is also noteworthy. As can be seen in Figure 9 (bottom), the phosphorus substituents closely approximate an idealized staggered conformation, with torsion angles of 53.48 to 57.14° (vs. 60°). The corresponding torsion angles in the other complexes are much smaller. The remaining two macrocycles in *trans*-**15e** exhibit spiral-staircase-like conformations that span two *gauche* positions. One features a much higher proportion of *gauche* segments than the ring analyzed above (8 of 17), apropos to the chiral and helical nature of such constructs. This underscores the conformational variability of the stators, especially as the lengths of the methylene chains are increased.

Cage dimensions and dynamic properties

The ultimate objective of this research is to prepare transition-metal-based gyroscope-like rotors in which the rotators can turn within cage like stators with energy barriers that are as low as possible. Towards this end, the interior space available within the stator as compared to the sizes of the rotor ligands is important. Figure 11 provides a starting point for a simple, but admittedly approximate, analysis that uses the preceding crystallographic data.

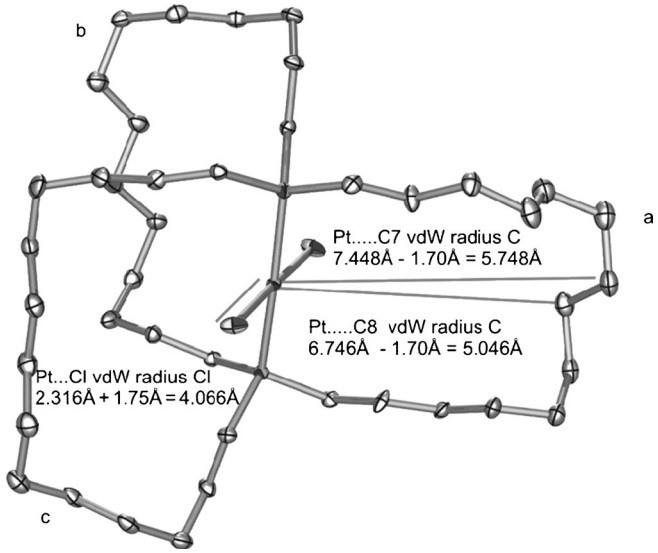

Figure 11. Calculations involving the spatial void between the rotator and the carbon spokes, illustrated using *trans*-**4c** as a model; a, b, c = corresponding macrocycles, vdW = van der Waals.

The first step is to calculate the radius of the rotator. For the dihalide complexes, this entails summing the average M–X bond lengths and the van der Waals radius of X.[38] For the bis(isothiocyanide) complex *trans*-**13c**, this entails summing the platinum–sulfur distance and the van der Waals radius of sulfur. For the diphenyl complexes *trans*-**15c**,**e**, the distance from platinum to the *para*-hydrogen atom is calculated, and the van der Waals radius of hydrogen is added. Values are presented in Table 5.

The horizontal interior space of the stator cage is then analyzed. First the distances between the metal atom and the remote carbon atoms of each macrocycle are calculated (C7

and C8 for $P(CH_2)_{14}P$ linkages). These are normally the two closest to the plane that would be defined by MX_2 rotation. As depicted in Figure 11 and summarized in Table 5, the distances vary, and the shortest among the six possibilities is taken. The van der Waals radius of an sp^3-hybridized carbon atom is then subtracted, giving a "horizontal clearance" or minimum "bridge height". The resulting distances ($M{-}C_{distal\text{-}vdW}$) are listed in Table 5. However, it should be emphasized that an equilibrium ensemble of macrocycle conformations would be expected in solution, and any impression of a rigid steric barrier is unintended.

The minimum "bridge heights" for the six dihalide complexes range from 3.734 to 3.935 Å, and the radii of the rotators range from 4.053 to 4.592 Å. In all cases the latter are somewhat greater. The radius of the rotators in the dicyanide complexes can be estimated as 4.68–4.69 Å from other crystallographically characterized platinum and palladium bis(phosphine) adducts.[39] Nonetheless, the $^{13}C\{^1H\}$ NMR data for all of these complexes show that rotation is rapid on the NMR timescale, even at low temperatures. Presumably, the passage of the MX_2 ligands through the macrocycles is correlated with conformational changes that enhance the horizontal clearance. As an upper bound on clearance, the longest of the six metal–carbon distances noted above is taken, and the van der Waals radius of a carbon atom subtracted ($M{-}C_{distal'\text{-}vdW}$). These values, 5.593 to 5.753 Å (Table 5), easily exceed the radii of the rotators.

A related issue involves the "floor-to-ceiling" or vertical interior space of the stator cage. Although the P–M–P distances present a possible starting point for analysis, we prefer to focus on the closest CH_2–P···P–CH_2 spacings (i.e., those associated with the smallest torsion angles, which are typically 34.8° to 52.2°). Consider the CH_2–P···P–CH_2 linkage in the platinum dichloride complex *trans*-**4c** that has a torsion angle of 37.9°. This corresponds to a carbon–carbon distance of 6.22 Å. When *twice* the van der Waals radius of carbon is subtracted, a rough floor-to-ceiling or vertical clearance of 2.82 Å is obtained. Importantly, this is less than the van der Waals diameter of a chlorine atom ($2\times1.75=3.50$ Å).[38] The fit becomes tighter for a larger iodide ligand ($2\times1.98=3.96$ Å), but is comparable for a cyanide ligand, for which the "width" can be approximated as twice the van der Waals radii of sp-hybridized nitrogen and carbon atoms ($2\times1.55=3.10$ Å, $2\times1.78=3.56$ Å).

With the bis(isothiocyanide) complex *trans*-**13c**, the radius of the rotator is substantially greater than the horizontal clearance (6.508 vs. 4.301 Å; Table 5). Thus, MX_2 rotation is effectively braked, and two sets of ^{13}C NMR signals are observed for the methylene carbon atoms. The same holds for the diphenyl complex *trans*-**15c** (7.083 vs. 3.506 Å), although the clearance afforded by the macrocycle with the extended *anti* segments (vide supra; P1 to C6A and C9A to P2) is much greater (6.090 Å). With the diphenyl complex *trans*-**15e**, which features 21-membered macrocycles, the horizontal clearance (4.215 Å) is set by one of the "spiral staircase" methylene chain motifs noted above. This would also seemingly brake $PtPh_2$ rotation, but rotation is fast for this complex. Importantly, the clearance afforded by the macrocycle with the extended *anti* segments (P1 to C8A; C11A to P2) is more than twice as great (8.786 Å). This suggests that as the macrocycles become larger, the radius of the rotator might better be compared to the average clearance of the three macrocycles.

Only non-hydrogen atoms of the stator have been considered in this admittedly qualitative analysis. As a partial justification, many conformational processes readily take place in organic molecules despite van der Waals interactions involving hydrogen atoms and/or difficulties executing them with space-filling models. Nonetheless, space-filling representations that include hydrogen atoms are provided in Figure 12 for the platinum dichloride, dibromide, and diiodide complexes *trans*-**4c**, *trans*-**7c**, and *trans*-**9c**. Visually the void spaces are modest, especially as compared to the larger iodide ligands in *trans*-**9c**. This underscores the necessity of coupling conformational processes involving the macrocycles to MX_2 rotation. Some space filling representations of *trans*-**15c** and *trans*-**15e** are provided in Figure 13. The last view highlights the thin space through which a phenyl ring must pass.

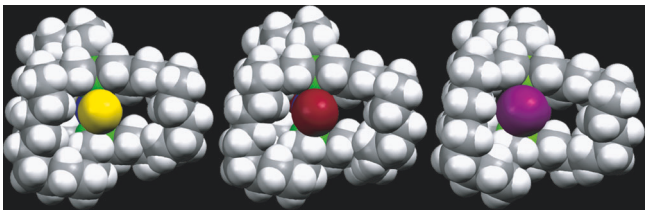

Figure 12. Space filling representations of *trans*-**4c**, *trans*-**7c** and *trans*-**9c**.

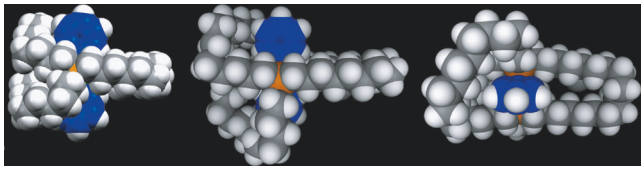

Figure 13. Space filling representations of *trans*-**15c**·*n*-C_5H_{12} (left, with solvent molecule omitted) and *trans*-**15e** (middle) along the P-Pt-P axes, and of *trans*-**15e** (right) along the C-Pt-C axis.

The new MCl_2, MBr_2, MI_2, and $M(CN)_2$ complexes appear to have considerably lower rotational barriers than their $Fe(CO)_3$ and $[Fe(CO)_2(NO)]^+$ analogues ($\Delta H^{\neq}$ 9.5 kcal mol^{-1}, $\Delta S^{\neq}$ −6.5 eu for the cation).[6] In another study involving the same diphosphine stator, a trivalent trigonal rhodium rotator ($Rh(CO)_2I$) was shown to have a distinctly higher rotational barrier than a divalent linear rhodium rotator (Rh(CO)I). This can be rationalized in the context of Scheme 5. A 360° rotation of a trigonal rotator would require three **IX** transition states with threefold eclipsing interactions. All three macrocycles must extend to accommodate the three eclipsed ligands. On the other hand, a 360° rotation of a divalent linear rotator would require six **VII** transition states with onefold eclipsing interactions. Only one macrocycle must be sufficiently extended. It is furthermore well established that in purely organic molecules,

sixfold rotational barriers are generally much lower than threefold rotational barriers.[40]

One must be mindful that mechanisms other than ML_2 rotation may render the methylene bridges equivalent on NMR timescales. NMR evidence against ligand dissociation was presented in the Results section. However, *cis*/*trans* isomerization about the metal also presents possibilities. Consider the isomer *cis*-**4c** shown in Scheme 10, which can be accessed by

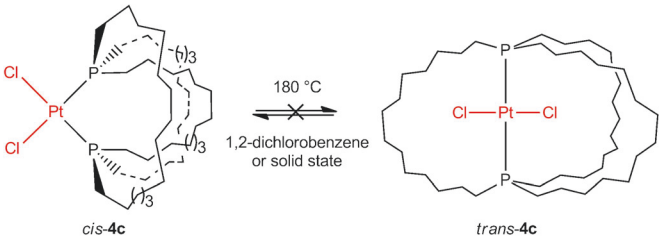

Scheme 10. Attempted equilibration of *cis*-**4c** and *trans*-**4c**.

a threefold intramolecular ring-closing metathesis of *cis*-**1c**. One macrocycle lies roughly in the platinum square plane, and the others above and below. In principle, these may exchange by a "jump rope" mechanism. However, *cis*-**4c** and *trans*-**4c** do not readily interconvert, either in solution or the solid state.

Structural data: lattice properties

Another question is whether the MX_2 moieties in the dihalide complexes might be able to rotate in the crystal lattice without interference from nearby molecules. Accordingly, for each complex the atom from a neighboring molecule closest to the metal was identified. These proved to be carbon atoms associated with macrocycles that intercalate between those of the reference molecule. The distances are summarized in Table 5 ($M–C_{neighbor}$, 4.619 to 5.878 Å), and increase monotonically with halide ligand size. The van der Waals radius of carbon was subtracted to give the corresponding clearances ($M–C_{neighbor-vdW}$, 2.919 to 4.178 Å). These were always much less than the radii of the respective rotors (4.053–4.592 Å). Hence, rotation can be considered blocked in the crystal lattice. The same holds for the other complexes in Table 5.

In this context, note that the conformational reorganization of the macrocycles necessary to sterically accommodate the passage of the rotator should require significantly more energy in the solid state than in solution. This might be facilitated by a phase transition corresponding to a disordering of the methylene chains. DSC data (Experimental Section) do reveal five complexes for which a melting endotherm is accompanied by a second lower temperature endotherm. However, crystal structures determined above and below the transition temperature did not reveal any new disorder, and these phenomena remain under investigation.

As can be seen in Table 2, the dichloride complexes *trans*-**4c** and *trans*-**5c** and dibromide complexes *trans*-**7c** and *trans*-**8c** crystallize in identical space groups ($P2_1/n$) with similar lattice constants ($Z=4$, $V=4454.1(16)$–$4510.31(14)$ and $4579.4(2)$–$4512(3)$ Å^3). The diiodide complexes *trans*-**9c** and *trans*-**10c** also crystallize in the same space group (*Pbca*) with very similar lattice constants ($Z=8$, $V=9507(3)$–$9469(3)$ Å^3). In all cases, the orientations of the P-M-P axes are of interest.

In the dichloride and dibromide complexes, there are two "non-parallel" sets of molecules with parallel P-M-P axes. A packing diagram illustrating this feature is given in Figure 14. The angle between the sets of axes can be quantified in several ways. One approach is to define a least-squares plane consisting of the six atoms of two parallel P-M-P axes of one set, and the analogous plane of the other set (this avoids dealing with the imprecise planes defined by three nearly collinear points). Alternatively, the least-square planes defined by the five-atom coordination planes (P-MX_2-P) may be employed. As summarized in Table 5, these values are in good agreement, and range from 78.07 to 79.87°.

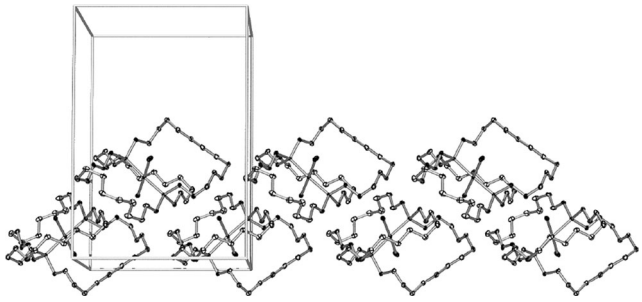

Figure 14. Packing diagram of *trans*-**5c** illustrating the two "non-parallel" sets of molecules with parallel P-M-P axes.

In the diiodide complexes, which have larger unit cells, there are four "non-parallel" sets of molecules with parallel P-M-P axes. Least-squares planes may be analogously defined, but the multiple angles generated are not tabulated. These diverse lattice geometries provide thought-provoking conceptual relationships to various macroscopic devices that are based upon multiple gyroscopes,[41] some of which feature non-parallel axes.

In the other crystallographically characterized complexes, *trans*-**13c** (space group $C2/c$, $Z=4$) and *trans*-**15c,e** (both space group $P\bar{1}$, $Z=4$), all P-Pt-P axes are parallel. However, most square-planar complexes crystallize with "non-parallel" sets of molecules with parallel P-M-P axes. Interestingly, trigonal bipyramidal gyroscope-like complexes tend to crystallize with parallel M-P-M axes. Also, in many cases the rotator can in principle rotate in the solid state without van der Waals interactions with a neighboring molecule. Examples include $[Fe(CO)_3(P\{(CH_2)_{14}\}_3P)]$,[6] analogues with different diphosphine ligands or osmium, and carbonyl ligand substitution products.[34b,42]

Towards molecular gyroscopes

Ideally, one would like to engineer stators that enclose their rotators in frictionless environments, both in solution and the

crystal lattice. The preceding structural analyses reveal some of the strengths and weaknesses of the square-planar systems reported herein. The "horizontal clearance" can be optimized by varying the sizes of the ligands on the rotator and the lengths of the methylene chains in the stator. The replacement of some methylene groups by more rigid units may also provide benefits.

However, there is much less flexibility with respect to the top/bottom or "vertical clearance". Towards this end, we recently prepared diarsine analogues of the iron diphosphine systems **III** in Scheme 1. Since iron–arsenic bonds are about 4% longer than iron–phosphorus bonds, the length of the axis is increased. However, additional progress will require spacer groups. One possibility would be an axis composed of a PAuC≡CM(L_2)C≡CAuP linkage.

From the standpoint of minimizing intermolecular interactions in the solid state, equatorial "belts" as found in most toy gyroscopes may prove useful. One approach would entail switching to alkyne metathesis for macrocyclization, the feasibility of which has been established for *trans*-phosphine ligands of the type $Ph_2P(CH_2)_mC{\equiv}CCH_3$.[43] The C≡C linkages could then be used for binding additional metals and possibly attendant bridging groups.

Regardless of the MX_2 rotational barriers associated with the preceding complexes, the MX_2 moieties of individual molecules would exhibit both clockwise and counterclockwise (i.e., Brownian) rotation. However, in order to attain gyroscopic properties, unidirectional rotation is required. One strategy for controlling the direction of a rotator involves introducing a dipole moment, such that it can be oriented by a static applied electric field or driven by a rotating electric field.[4,44] Both substitution reactions of the types in Schemes 3 and 4, and ring-closing metatheses of less symmetrical substrates—such as rhodium carbonyl chloride analogues of the preceding dichloride complexes (see **IV**, Scheme 1)[9]—should provide practical routes to such species.

Conclusion

We have demonstrated that it is possible to 1) enclose rotators of the formula $PdCl_2$ and $PtCl_2$ in *trans*-spanning diphosphine ligands using threefold intramolecular alkene metatheses, 2) elaborate the caged rotators through substitution reactions, and 3) extrude the rotators from the diphosphines. All of these steps pose fascinating mechanistic questions, which remain under investigation. Consistent with certain design elements, the MCl_2, MBr_2, MI_2, and $M(CN)_2$ complexes appear to have considerably lower rotational barriers than their $Fe(CO)_3$ and $[Fe(CO)_2(NO)]^+$ analogues.[6] Attempts to quantify these remain in progress. Regardless, the barriers are increased when the sizes of the ligands are increased to isothiocyanide and phenyl, and can be modulated by varying the lengths of the methylene bridges. Current efforts are directed at the synthesis of analogues with 1) more spacious stators, and 2) unsymmetrically substituted rotators (MXX′). The dipole moments of the latter should be responsive to external electric fields, providing a means of orienting the rotators or driving unidirectional rotation, as in compasses and gyroscopes.

Experimental Section

General: Except for hydrogenations, reactions were conducted under dry inert atmospheres. Chemicals were treated as follows: THF, benzene, toluene, hexanes, and pentane, distilled from Na/benzophenone or Na; acetone, distilled from $CaCl_2$; CH_2Cl_2 and $CDCl_3$, distilled from CaH_2; CH_2Cl_2 (for workups) and CH_3OH, simple distillation; NaC≡CH (Acros, 18 wt% slurry in xylene), used as received or isolated by filtration, washed with toluene under argon, and dried in vacuo (18 h); Grubbs' catalyst ($[(Cy_3P)_2Cl_2Ru(=CHPh)]$; Aldrich), $[RhCl(PPh_3)_3]$ (97%, Alfa Aesar or Strem), LiBr (Fluka, 99%), NaI (Rienst, 99%), KCN, KSCN (2×Fluka, 98%), Ph_2Zn (Acros, 98%), $BH_3{\cdot}S(CH_3)_2$ (2.0 M in THF, Acros), used as received.

NMR spectra were recorded on 500–300 MHz spectrometers and referenced as follows: ^{1}H: residual internal $CHCl_3$ (δ, 7.24 ppm); ^{13}C: internal $CDCl_3$ (δ, 77.0 ppm); ^{31}P: external H_3PO_4 ($\delta = 0.00$ ppm). IR spectra were recorded using ATR accessories. DSC and TGA data were treated by standard methods.[45] Instrument models and related details are provided in the Supporting Information of earlier papers.[7,30,31]

***trans*-[PtCl$_2$(P{(CH$_2$)$_{14}$}$_3$P)] (*trans*-4c) and *trans*-[PtCl$_2$({P(CH$_2$)$_{14}$}-(CH$_2$)$_{14}$P{(CH$_2$)$_{14}$})] (*trans*-4′c)**

Method A: A two-necked flask was charged with *trans*-**1c**[19] (1.000 g, 1.005 mmol) and CH_2Cl_2 (285 mL; the resulting solution was 0.0035 M in *trans*-**1c**), and fitted with a condenser with a bubbler. The solution was cooled to 0 °C. A solution of Grubbs' catalyst (0.0251 g, 0.0305 mmol, 3.0 mol%) in CH_2Cl_2 (50 mL) was added dropwise over 100 min.[46] The solution was refluxed (16 h), cooled, and passed through a pad of neutral alumina (3×10 cm, rinsed with CH_2Cl_2). The filtrate was concentrated to about 10 mL. A Fischer–Porter bottle was charged with the filtrate and $[RhCl(PPh_3)_3]$ (0.1202 g, 0.1299 mmol), and flushed and pressurized with H_2 (5 bar). The solution was stirred at 45 °C. After 4 d, the solvent was removed by rotary evaporation. The residue was passed through a pad of neutral alumina (2.5×7.0 cm, rinsed with CH_2Cl_2). The solvent was removed from the filtrate by rotary evaporation. The residue was subjected to chromatography on a silica column (3.5×14 cm, 1:2 v/v CH_2Cl_2/hexanes). The solvent was removed from the product fraction by rotary evaporation to give *trans*-**4c** as a pale yellow waxy oil, which solidified after 15 min (0.398 g, 0.434 mmol, 43%).

M.p. (capillary) 116–117 °C; DSC ($T_i/T_e/T_p/T_f$): 77.8/114.7/118.0/126.3 °C (endotherm); TGA: onset of mass loss, 284 °C; elemental analysis calcd (%) for $C_{42}H_{84}Cl_2P_2Pt$: C 55.01, H 9.23; found: C 54.81, H 9.22; ^{1}H NMR ($CDCl_3$):[47] $\delta = {}^1$H 1.95–1.80 (br m, 12H; PCH_2), 1.80–1.60 (br m, 12H; PCH$_2$CH_2), 1.50–1.38 (br m, 12H; PCH$_2$CH$_2$CH_2), 1.38–1.20 ppm (br m, remaining CH_2); ^{13}C{^{1}H} NMR: $\delta = 30.0$ (virtual t,[23] $^3J_{CP} = 6.8$ Hz, PCH$_2$CH$_2$CH_2), 28.1 (s, CH_2), 27.1 (s, 2CH_2), 26.8 (s, CH_2), 23.1 (s, PCH$_2$CH_2), 21.3 ppm (virtual t,[23] $^1J_{CP} = 16.3$ Hz, PCH_2); ^{31}P{^{1}H} NMR: $\delta = 7.1$ ppm (s, $^1J_{PPt} = 2398$ Hz).[48] IR (powder film): $\tilde{\nu} = 2922$ (s), 2851 (s), 1461 (m), 1411 (s), 1351 (s), 1261 (s), 1106 (s), 1005 (s), 820 (s), 795 (m), 719 cm^{-1} (m); MS:[49a] *m/z* (%): 917 (100) $[M]^+$, 882 (50) $[M-Cl]^+$.

Method B: Five two-necked round-bottomed flasks were charged with *trans*-**1c** (**i–v**: 2×1.903 g, 2×1.912 mmol; 2×2.141 g, 2×2.151 mmol; 1.843 g, 1.852 mmol), CH_2Cl_2 (**i–v**: 2×1000 mL, 2×1200 mL, 1000 mL) and cooled to 0 °C. Solutions of Grubbs' catalyst (**i–v**: 0.051 g, 0.062 mmol, 3 mol%; 0.056 g, 0.068 mmol, 4 mol%; 2×0.107 g, 2×0.130 mmol, 2×6 mol%; 0.092 g, 0.112 mmol,

6 mol%;) in CH_2Cl_2 (**i**–**v**: 250 mL, 200 mL, 3×30 mL) were added dropwise over 90–15 min, respectively. The cooling baths were removed, and the flasks were fitted with condensers with bubblers. The mixtures were refluxed (4–8 d). Runs **i**, **ii**, and **iv** were charged with a second portion of Grubbs' catalyst (**i**: 0.050 g, 0.061 mmol, 3 mol%, **ii**: 0.051 g, 0.062 mmol, 3 mol%, and **iv**: 0.109 g, 0.132 mmol, 6 mol%) and refluxed (1–6 d additional). The mixtures were cooled to room temperature, exposed to air (3–7 d), and passed through pads of neutral alumina (4 cm) that were rinsed with CH_2Cl_2. The filtrates were concentrated to about 30 mL. Five Fischer–Porter bottles were charged with $[RhCl(PPh_3)_3]$ (**i**: 0.088 g, 0.095 mmol, 5 mol%; **ii**: 0.089 g, 0.096 mmol, 5 mol%; **iii**: 0.120 g, 0.130 mmol, 6 mol%; **iv**: 0.119 g, 0.129 mmol, 6 mol%; **v**: 0.104 g, 0.112 mmol, 6 mol%) and the concentrates, and then flushed and pressurized with H_2 (5 bar). The mixtures were stirred at 40 °C (4–6 d), and the solvents were removed by rotary evaporation. The residues were combined and placed at the top of a silica column (10 cm) that was eluted with hexanes/CH_2Cl_2 (1:0 to 0:1 v/v). The solvents were removed from the product containing fractions by rotary evaporation and oil pump vacuum to give *trans*-**4c** (2.895 g, 3.157 mmol, 32%; eluting first) as a yellowish solid and *trans*-**4′c** (0.498 g, 0.543 mmol, 5%) as a yellowish viscous oil.

Data for trans-***4′c***: Elemental analysis calcd (%) for $C_{42}H_{84}P_2PtCl_2$: C 55.01, H 9.23; found: C 55.13, H 9.45; ^{1}H NMR ($CDCl_3$): δ = 2.01–1.95 (m, 4H; CH_2), 1.88–1.56 (m, 16H; CH_2), 1.48–1.14 ppm (m, 64H; CH_2); $^{13}C\{^1H\}$ NMR: δ = 31.3 (virtual t, J_{CP} = 7.3 Hz, $PCH_2CH_2CH_2$), 29.0 (virtual t, J_{CP} = 6.2 Hz, $2PCH_2CH_2CH_2$), 28.1 (s, CH_2), 27.2 (s, CH_2), 26.87 (s, CH_2), 26.84 (s, $2CH_2$), 26.77 (s, $2CH_2$), 26.65 (s, $2CH_2$), 26.2 (s, $2CH_2$), 25.4 (s, CH_2), 24.9 (s, CH_2), 23.1 (virtual t, J_{CP} = 16.3 Hz, PCH_2), 21.7 (s, PCH_2CH_2), 18.9 ppm (virtual t, J_{CP} = 15.9 Hz, $2PCH_2$); $^{31}P\{^1H\}$ NMR: δ = 5.6 ppm (s, $^1J_{PPt}$ = 2374 Hz);[48] MS:[49b] *m/z* (%): 881.5 (2) $[M-Cl]^+$, 651.6 (3) $[M-PtCl_2]^+$, 326.3 (100) $[M-PtCl_2+H]^{2+}$.

***trans*-[PtCl$_2$(P{(CH$_2$)$_{16}$}$_3$P)] (*trans*-4d) and *trans*-[PtCl$_2$({P(CH$_2$)$_{16}$}-(CH$_2$)$_{16}$P{(CH$_2$)$_{16}$})] (*trans*-4′d)**

Method A: A two-necked flask was charged with *trans*–**1d**[19] (0.522 g, 0.484 mmol) and CH_2Cl_2 (250 mL; the resulting solution was 0.0019 M in *trans*-**1d**), and fitted with a condenser with a bubbler. The solution was cooled to 0 °C. A solution of Grubbs' catalyst (0.0141 g, 0.0171 mmol, 3.5 mol%) in CH_2Cl_2 (15 mL) was added dropwise over 1 h.[44] The solution was refluxed (17 h). The mixture was cooled and passed through a pad of neutral alumina (1.5×7.0 cm, rinsed with CH_2Cl_2). The filtrate was concentrated to about 5 mL. A Fischer–Porter bottle was charged with the filtrate and $[RhCl(PPh_3)_3]$ (0.0652 g, 0.0705 mmol), and flushed and pressurized with H_2 (5 bar). The solution was stirred at 50 °C. After 4 d, the solvent was removed by rotary evaporation. The residue was passed through a pad of neutral alumina (1.5×15 cm, rinsed with CH_2Cl_2). The solvent was removed from the filtrate by rotary evaporation. The residue was subjected to chromatography on a silica column (3×24 cm, 1:6 v/v CH_2Cl_2/hexanes). The solvent was removed from the product fraction by rotary evaporation to give *trans*-**4d** as a pale yellow waxy oil, which solidified after 24 h (0.0172 g, 0.0172 mmol, 4%).

Elemental analysis calcd (%) for $C_{48}H_{96}Cl_2P_2Pt$: C 57.58, H 9.66; found: C 58.20, H 10.05;[50] ^{1}H NMR ($CDCl_3$):[51] δ = 1.90–1.70 (br m, 12H; PCH_2), 1.70–1.52 (br m, 12H; PCH_2CH_2), 1.48–1.36 (br m, 12H; $PCH_2CH_2CH_2$), 1.36–1.20 ppm (br m, remaining CH_2); $^{13}C\{^1H\}$ NMR: δ = 31.4 (virtual t,[23] $^3J_{CP}$ = 6.7 Hz, $PCH_2CH_2CH_2$), 28.2 (s, CH_2), 27.9 (s, CH_2), 27.8 (s, CH_2), 27.7 (s, CH_2), 27.4 (s, CH_2), 23.2 (s, PCH_2CH_2), 20.8 ppm (virtual t,[23] $^1J_{CP}$ = 16.2 Hz, PCH_2); $^{31}P\{^1H\}$ NMR: δ = 6.0 ppm (s, $^1J_{PPt}$ = 2398 Hz);[48] IR (powder film): $\tilde{\nu}$ = 2922 (s), 2853 (s), 1459 (m), 1413 (m), 1351 (w), 1100 (w), 1054 (w), 1019 (w), 791 (m), 752 (m), 718 cm^{-1} (m); MS:[49a] *m/z* (%): 1000 (55) $[M]^+$, 964 (50) $[M-Cl]^+$, 928 (100) $[M-2Cl]^+$.

Method B: Complex *trans*-**1d** (0.609 g, 0.564 mmol), CH_2Cl_2 (230 mL; the resulting solution was 0.0025 M in *trans*-**1d**), and Grubbs' catalyst (0.0144 g, 0.0175 mmol, 3.1 mol%) in CH_2Cl_2 (11 mL) were combined as in procedure A. The solution was refluxed (18 h). The mixture was cooled and passed through a pad of neutral alumina (2.5×5 cm, rinsed with CH_2Cl_2). The filtrate was concentrated to about 7 mL. A Fischer–Porter bottle was charged with the filtrate and $[RhCl(PPh_3)_3]$ (0.0754 g, 0.0815 mmol), and flushed and pressurized with H_2 (5 bar). The solution was stirred at 45 °C. After 4 d, the solvent was removed by rotary evaporation. The residue was passed through a pad of neutral alumina (2.5×5 cm, rinsed with CH_2Cl_2). The solvent was removed from the filtrate by rotary evaporation. The residue was subjected to chromatography on a silica column (2×24 cm, 1:6 v/v CH_2Cl_2/hexanes). The solvent was removed from the product fraction by rotary evaporation to give *trans*-**4′d** as a pale yellow waxy oil, which solidified after 24 h (0.0208 g, 0.0208 mmol, 4%).

M.p. (capillary) 59–60 °C; DSC ($T_i/T_e/T_p/T_c/T_f$): 36.2/64.4/73.4/78.9/103.4 °C (endotherm); 190.1/221.9/260.0/279.9/289.8 °C (exotherm); TGA: onset of mass loss, 282 °C; elemental analysis calcd (%) for $C_{48}H_{96}Cl_2P_2Pt$: C 57.58, H 9.66; found: C 57.27, H 9.66; ^{1}H NMR ($CDCl_3$): δ = 2.19–2.01 (br m, 4H; CH_2), 1.79–1.67 (br m, 8H; CH_2), 1.66–1.55 (br m, 8H; CH_2), 1.46–1.36 (br m, 16H; CH_2), 1.41–1.22 ppm (br m, 60H; CH_2); $^{13}C\{^1H\}$ NMR: δ = 31.6 (virtual t,[23] J_{CP} = 7.2 Hz, $PCH_2CH_2CH_2$), 29.9 (virtual t,[23] J_{CP} = 6.3 Hz, $2PCH_2CH_2CH_2$), 29.7 (s, CH_2), 28.9 (s, CH_2), 28.2 (s, CH_2), 27.83 (s, $2CH_2$), 27.76 (s, CH_2), 27.6 (s, $2CH_2$), 27.5 (s, $2CH_2$), 27.4 (s, $2CH_2$), 27.0 (s, $2CH_2$), 26.8 (s, CH_2), 26.3 (s, CH_2), 25.0 (s, CH_2), 22.8 (center of obscured virtual t,[23] $^1J_{CP}$ = 16.1 Hz, PCH_2), 22.6 (s, PCH_2CH_2), 19.2 ppm (virtual t,[23] J_{CP} = 16.0 Hz, $2PCH_2$); $^{31}P\{^1H\}$ NMR: δ = 5.5 ppm (s, $^1J_{PPt}$ = 2374 Hz);[48] IR (powder film): $\tilde{\nu}$ = 2921 (s), 2852 (s), 1459 (m), 1414 (w), 1351 (w), 1202 (w), 1050 (m), 795 (m), 725 (m), 718 cm^{-1} (m); MS:[49a] *m/z* (%): 1000 (45) $[M]^+$, 965 (50) $[M-Cl]^+$.

***trans*-[PtCl$_2$(P{(CH$_2$)$_{18}$}$_3$P)] (*trans*-4e) and *trans*-[PtCl$_2$({P(CH$_2$)$_{18}$}-(CH$_2$)$_{18}$P{(CH$_2$)$_{18}$})] (*trans*-4′e)**: The complex *trans*-**1e**[19] (0.750 g, 0.645 mmol), CH_2Cl_2 (650 mL; the resulting solution was 0.0010 M in *trans*-**1e**), and a solution of Grubbs' catalyst (0.0181 g, 0.0220 mmol, 3.0 mol%) in CH_2Cl_2 (25 mL) were combined as in method A for *trans*-**4d**. The solution was refluxed (20 h). The mixture was cooled and passed through a pad of neutral alumina (2.5×5 cm, rinsed with CH_2Cl_2). The filtrate was concentrated to about 5 mL. A Fischer–Porter bottle was charged with the filtrate and $[RhCl(PPh_3)_3]$ (0.0904 g, 0.0977 mmol), and flushed and pressurized with H_2 (5 bar). The solution was stirred at 50 °C. After 4 d, the solvent was removed by rotary evaporation. The residue was passed through a pad of neutral alumina (2×5 cm, rinsed with CH_2Cl_2). The solvent was removed from the filtrate by rotary evaporation. The residue was subjected to chromatography on a silica column (3×22 cm, 1:8 v/v CH_2Cl_2/hexanes). The solvent was removed from the product fractions by rotary evaporation to give *trans*-**4e** as a pale yellow waxy oil, which solidified after 24 h (0.1991 g, 0.1834 mmol, 28%, R_f = 0.68), and *trans*-**4′e** as a pale yellow waxy oil, which solidified after 72 h (0.1612 g, 0.1485 mmol, 23%, R_f = 0.57).

Data for trans-***4e***: M.p. (capillary) 48–50 °C; DSC ($T_i/T_e/T_p/T_c/T_f$): 35.6/49.1/52.3/55.4/68.8 °C (endotherm); TGA: onset of mass loss, 330 °C; elemental analysis calcd (%) for $C_{54}H_{108}Cl_2P_2Pt$: C 59.76, H 10.03; found: C 59.54, H 9.74; ^{1}H NMR ($CDCl_3$):[51] δ = 1.83–1.80 (br m, 12H; PCH_2), 1.60–1.57 (br m, 12H; PCH_2CH_2), 1.42–1.38 (br m, 12H; $PCH_2CH_2CH_2$), 1.38–1.27 ppm (br m, remaining CH_2); $^{13}C\{^1H\}$ NMR: δ = 30.7 (virtual t,[23] $^3J_{CP}$ = 6.6 Hz, $PCH_2CH_2CH_2$), 28.5 (s, CH_2),

28.3 (s, CH_2), 28.2 (s, $2CH_2$), 27.9 (s, CH_2), 27.6 (s, CH_2), 23.4 (s, PCH_2CH_2), 20.7 ppm (virtual t,[23] $^1J_{CP}=16.2$ Hz, PCH_2); $^{31}P\{^1H\}$ NMR: 6.5 ppm (s, $^1J_{PPt}=2389$ Hz);[48] IR (powder film): $\tilde{\nu}=2922$ (s), 2853 (s), 1459 (m), 1417 (w), 1351 (w), 1124 (w), 1083 (w), 1061 (w), 791 (m), 718 cm^{-1} (m); MS:[49a] *m/z* (%): 1084 (40) $[M]^+$, 1048 (45) $[M-Cl]^+$.

Data for trans-***4′e***: DSC ($T_i/T_e/T_p/T_c/T_f$): 36.5/60.8/68.1/73.7/93.5 °C (endotherm); 214.2/230.4/247.3/262.3/294.4 °C (exotherm); TGA: onset of mass loss, 291 °C; elemental analysis calcd (%) for $C_{54}H_{108}Cl_2P_2Pt$: C 59.76, H 10.03; found: C 59.30, H 10.04; ^1H NMR ($CDCl_3$): $\delta=2.05$–1.85 (br m, 4H; CH_2), 1.85–1.70 (br m, 4H; CH_2), 1.70–1.52 (br m, 10H; CH_2), 1.48–1.30 (br m, 20H; CH_2), 1.35–1.15 ppm (br m, 70H; CH_2); $^{13}C\{^1H\}$ NMR: $\delta=31.4$ (virtual t,[23] $J_{CP}=6.8$ Hz, $PCH_2CH_2CH_2$), 30.6 (virtual t,[23] $J_{CP}=6.2$ Hz, $2PCH_2CH_2CH_2$), 29.2 (s, CH_2), 28.9 (s, CH_2), 28.4 (s, $2CH_2$), 28.3 (s, $2CH_2$), 28.2 (s, CH_2), 28.1 (s, $2CH_2$), 28.0 (s, $2CH_2$), 27.6 (s, $2CH_2$), 27.5 (s, CH_2), 27.4 (s, CH_2), 27.3 (s, $2CH_2$), 26.6 (s, CH_2), 24.7 (s, CH_2), 22.8 (s, PCH_2CH_2), 22.6 (partially obscured virtual t,[23] $J_{CP}=16.5$ Hz, PCH_2), 19.3 ppm (virtual t,[23] $J_{CP}=16.0$ Hz, $2PCH_2$); $^{31}P\{^1H\}$ NMR: $\delta=5.4$ ppm (s, $^1J_{PPt}=2374$ Hz);[48] IR (powder film): $\tilde{\nu}=2922$ (s), 2853 (s), 1459 (m), 1413 (w), 1124 (w), 1058 (w), 1023 (w), 795 (m), 718 cm^{-1} (m); MS:[49a] *m/z* (%): 1084 (40) $[M]^+$, 1047 (45) $[M-Cl]^+$.

***trans*-[$\overline{PdCl_2(P\{(CH_2)_{14}\}_3P)}$] (*trans*-5c)**: The complex *trans*-**2c**[19] (0.450 g, 0.496 mmol), CH_2Cl_2 (140 mL; the resulting solution was 0.0035 M in *trans*-**2c**), and a solution of Grubbs' catalyst (0.0301 g, 0.0366 mmol, 7.4 mol%) in CH_2Cl_2 (40 mL) were combined as in method A for *trans*-**4d**. The solution was refluxed (12 h) and cooled to 0 °C. A second charge of Grubbs' catalyst (0.0251 g, 0.0305 mmol, 6.1 mol%) in CH_2Cl_2 (35 mL) was added dropwise over 1 h.[46] The solution was refluxed (15 h; $^{31}P\{^1H\}$ NMR (aliquot): $\delta=16.4$ (s), 15.0 (s), 13.6 (s) 13.0–11.9 ppm (broad oligomer signals)). The mixture was passed through a pad of neutral alumina (3×10 cm, rinsed with CH_2Cl_2). The filtrate was concentrated to about 5 mL. A Fischer–Porter bottle was charged with the filtrate and $[RhCl(PPh_3)_3]$ (0.0650 g, 0.0703 mmol), and flushed and pressurized with H_2 (5 bar). The solution was stirred at 55 °C. After 4 d, the solvent was removed by rotary evaporation. The residue was passed through two pads of neutral alumina (2×10 cm and 2×5 cm, rinsed with 1:1 v/v CH_2Cl_2/hexanes). The solvent was removed from the filtrate by rotary evaporation. The residue was subjected to chromatography on a neutral alumina column (3.5×26 cm, 1:9 v/v CH_2Cl_2/hexanes). The solvent was removed from the product fraction by rotary evaporation to give *trans*-**5c** as a yellow waxy oil, which solidified after 18 h (0.150 g, 0.181 mmol, 36%).

DSC ($T_i/T_e/T_p/T_f$): 73.9/99.8/111.1/117.8 °C (endotherm); TGA: onset of mass loss, 303 °C; elemental analysis calcd (%) for $C_{42}H_{84}Cl_2P_2Pd$: C 60.90, H 10.22; found: C 60.90, H 10.33; ^1H NMR ($CDCl_3$):[51] $\delta=$ 1.76–1.73 (br m, 12H; PCH_2), 1.73–1.56 (br m, 12H; PCH_2CH_2), 1.52–1.41 (apparent t, 12H; $PCH_2CH_2CH_2$), 1.41–1.14 ppm (br m, remaining CH_2); $^{13}C\{^1H\}$ NMR: $\delta=30.2$ (virtual t,[23] $^3J_{CP}=6.7$ Hz, $PCH_2CH_2CH_2$), 28.1 (s, CH_2), 27.2 (s, CH_2), 27.1 (s, CH_2), 26.9 (s, CH_2), 23.5 (s, PCH_2CH_2), 22.4 ppm (virtual t,[23] $^1J_{CP}=12.2$ Hz, PCH_2); $^{31}P\{^1H\}$ NMR: $\delta=13.3$ ppm (s); IR (powder film): $\tilde{\nu}=2921$ (s), 2850 (s), 1459 (m), 1409 (s), 1262 (m), 1094 (m), 1052 (m), 1015 (w), 791 (m), 714 cm^{-1} (m); MS:[49a] *m/z* (%): 827 (100) $[M]^+$, 791 (90) $[M-Cl]^+$, 755 (85) $[M-2Cl]^+$.

***trans*-[$\overline{PdCl_2(P\{(CH_2)_{18}\}_3P)}$] (*trans*-5e) and *trans*-[$\overline{PdCl_2(\{P(CH_2)_{18}\}(CH_2)_{18}P\{(CH_2)_{18}\})}$] (*trans*-5′e)**: The complex *trans*-**2e**[19] (0.900 g, 0.837 mmol), CH_2Cl_2 (590 mL; the resulting solution was 0.0014 M in *trans*-**2e**), and a solution of Grubbs' catalyst (0.0201 g, 0.0244 mmol, 2.9 mol%) in CH_2Cl_2 (45 mL) were combined as in method A for *trans*-**4d** (95 min addition time). The solution was refluxed (20 h) and cooled to 0 °C. A second charge of Grubbs' catalyst (0.0202 g, 0.0245 mmol, 2.9 mol%) in CH_2Cl_2 (45 mL) was added dropwise over 50 min.[46] The solution was refluxed (16 h; $^{31}P\{^1H\}$ NMR (aliquot): $\delta=13.5$ (s), 13.1 (s), 12.3 (s), 12.1 (s), 12.1–11.9 ppm (broad oligomer signals)). The mixture was passed through a pad of neutral alumina (3×5 cm, rinsed with CH_2Cl_2). The filtrate was concentrated to about 5 mL. A Fischer–Porter bottle was charged with the filtrate and $[RhCl(PPh_3)_3]$ (0.1101 g, 0.1190 mmol), and flushed and pressurized with H_2 (5 bar). The solution was stirred at 40 °C. After 4 d, the solvent was removed by rotary evaporation. The residue was passed through a pad of neutral alumina (2×5 cm, rinsed with 1:1 v/v CH_2Cl_2/hexanes). The solvent was removed from the filtrate by rotary evaporation. The residue was subjected to chromatography on a silica column (5.5×25 cm, 1:6 v/v CH_2Cl_2/hexanes). The solvent was removed from the product fractions by rotary evaporation to give *trans*-**5e** as a yellow waxy oil, which solidified after 4 d (0.1223 g, 0.1227 mmol, 15%, $R_f=0.43$), and *trans*-**5′e** as a yellow waxy oil, which solidified after 16 d (0.0225 g, 0.0226 mmol, 3%, $R_f=0.36$).

Data for trans-***5e***: M.p. (capillary) 56–57 °C; DSC ($T_i/T_e/T_p/T_f$): 34.4/53.2/58.8/70.2 °C (endotherm); TGA: onset of mass loss, 290 °C; elemental analysis calcd (%) for $C_{54}H_{108}Cl_2P_2Pd$: C 65.07, H 10.92; found: C 65.00, H 11.03; ^1H NMR (δ ($CDCl_3$):[51] $\delta=1.82$–1.75 (br m, 12H; PCH_2), 1.63–1.52 (br m, 12H; PCH_2CH_2), 1.46–1.38 (br m, 12H; $PCH_2CH_2CH_2$), 1.38–1.23 ppm (br m, remaining CH_2); $^{13}C\{^1H\}$ NMR: $\delta=30.8$ (virtual t,[23] $^3J_{CP}=6.6$ Hz, $PCH_2CH_2CH_2$), 28.5 (s, CH_2), 28.4 (s, CH_2), 28.3 (s, CH_2), 28.2 (s, CH_2), 27.7 (s, CH_2), 27.1 (s, CH_2), 23.9 (s, PCH_2CH_2), 21.7 ppm (virtual t,[23] $^1J_{CP}=13.1$ Hz, PCH_2); $^{31}P\{^1H\}$ NMR: $\delta=10.1$ ppm (s); IR (powder film): $\tilde{\nu}=2921$ (s), 2851 (s), 1461 (m), 1442 (m), 1350 (m), 1262 (m), 1098 (m), 1057 (s), 1039 (m), 1022 (m), 775 (m), 718 cm^{-1} (m); MS:[49a] *m/z* (%): 997 (70) $[M]^+$, 960 (80) $[M-Cl]^+$, 925 (40) $[M-2Cl]^+$.

Data for trans-***5′e***: DSC ($T_i/T_e/T_p/T_f$): 38.2/55.9/67.0/75.4 °C (endotherm); TGA: onset of mass loss, 293 °C; elemental analysis calcd (%) for $C_{54}H_{108}Cl_2P_2Pd$: C 65.07, H 10.92; found: C 65.14, H 10.96; ^1H NMR ($CDCl_3$): $\delta=2.03$–1.91 (br m, 4H; CH_2), 1.78–1.68 (br m, 4H; CH_2), 1.68–1.52 (br m, 10H; CH_2), 1.48–1.34 (br m, 20H; CH_2), 1.34–1.18 ppm (br m, 70H; CH_2); $^{13}C\{^1H\}$ NMR: $\delta=31.5$ (virtual t,[23] $J_{CP}=7.0$ Hz, $PCH_2CH_2CH_2$), 30.6 (virtual t,[23] $J_{CP}=6.1$ Hz, $2PCH_2CH_2CH_2$), 29.2 (s, CH_2), 28.9 (s, CH_2), 28.4 (s, $2CH_2$), 28.3 (s, $2CH_2$), 28.2 (s, CH_2), 28.1 (s, $2CH_2$), 28.0 (s, $2CH_2$), 27.6 (s, $2CH_2$), 27.45 (s, CH_2), 27.42 (s, CH_2), 27.3 (s, $2CH_2$), 26.6 (s, CH_2), 25.1 (s, PCH_2CH_2), 23.2 (s, $2PCH_2CH_2$), 20.5 ppm (virtual t,[23] $J_{CP}=12.8$ Hz, $2PCH_2$); $^{31}P\{^1H\}$ NMR:$\delta=11.0$ ppm (s); IR (powder film): $\tilde{\nu}=2921$ (s), 2852 (s), 1461 (m), 1412 (w), 1059 (w), 795 (m), 749 (m), 713 cm^{-1} (m); MS:[49a] *m/z* (%): 997 (70) $[M]^+$, 960 (80) $[M-Cl]^+$, 925 (40) $[M-2Cl]^+$.

***trans*-[$\overline{PdBr_2(P\{(CH_2)_{14}\}_3P)}$] (*trans*-8c)**

Method A: The complex *trans*-**3c**[19] (0.162 g, 0.163 mmol), CH_2Cl_2 (65 mL; the resulting solution was 0.0025 M in *trans*-**3c**), and a solution of Grubbs' catalyst (0.0140 g, 0.0170 mmol, 10 mol%) in CH_2Cl_2 (5 mL) were combined as in method A for *trans*-**4d** (95 min addition time). The solution was refluxed (15 h) and cooled to 0 °C. A second charge of Grubbs' catalyst (0.0141 g, 0. 0171 mmol, 10 mol%) in CH_2Cl_2 (5 mL) was added dropwise over 30 min.[46] The solution was refluxed (24 h; $^{31}P\{^1H\}$ NMR (aliquot): $\delta=15.51$ (s), 14.27 (s), 12.82 (s), 12.40–9.50 ppm (broad oligomer signals)). The mixture was cooled and passed through a pad of neutral alumina (1.5×10 cm, rinsed with CH_2Cl_2). The filtrate was concentrated to about 3 mL. A Fischer–Porter bottle was charged with the filtrate and $[RhCl(PPh_3)_3]$ (0.030 g, 0.032 mmol), and flushed and pressurized with H_2 (5 bar). The solution was stirred at 55 °C. After 92 h, the solvent was removed by rotary evaporation. The residue was passed through a pad of neutral alumina (2×7 cm, rinsed with 1:1 v/v CH_2Cl_2/hexanes). The solvent was removed from the filtrate by

rotary evaporation. The residue was subjected to chromatography on a neutral alumina column (1.5×15 cm, 1:1 v/v CH_2Cl_2/hexanes). The solvent was removed from the product fraction by rotary evaporation to give a yellow oil (mixture of *trans*-**5c**, *trans*-**6c** (Scheme 3), and *trans*-**8c**) that solidified after several days (0.0290 g, 0.0316 mmol,[52] 19%). $^{31}P\{^1H\}$ NMR ($CDCl_3$): $\delta = 13.3$ (s, 10%, **5c**), 12.2 (s, 50%, **6c**), 10.6 ppm (s, 40%, **8c**); MS:[49a] *m/z* (%): 916 (5) $[M]^+$, 872 (55) $[PdBrCl(P\{(CH_2)_{14}\}_3P)]^+$, 835 (60) $[PdBr(P\{(CH_2)_{14}\}_3P)]^+$, 791 (100) $[PdCl(P\{(CH_2)_{14}\}_3P)]^+$, 755 (100) $[Pd(P\{(CH_2)_{14}\}_3P)]^+$.

Method B: A 5 mm NMR tube was charged with *trans*-**5c** (0.0112 g, 0.0135 mmol) and THF (0.6 mL). Another NMR tube was charged with LiBr (0.0027 g, 0.031 mmol). The solution in the first tube was cannulated in stages into the second. After 30 min, a $^{31}P\{^1H\}$ NMR spectrum showed >99% conversion. The solvent was removed by oil pump vacuum. The residue was extracted with benzene. The solvent was removed from the extract by freeze pump drying to give *trans*-**8c** as a yellow powder (0.0123 g, 0.0134 mmol, 99%). M.p. (capillary) 112–114 °C; DSC ($T_i/T_e/T_p/T_f$): 77.2/106.0/114.0/123.1 °C (endotherm); TGA: onset of mass loss, 280 °C; elemental analysis calcd (%) for $C_{42}H_{84}Br_2P_2Pd$: C 54.99, H 9.23; found: C 54.17, H 8.99;[50] ^1H NMR ($CDCl_3$):[51] $\delta = 1.91$–1.88 (br m, 12H; PCH_2), 1.75–1.65 (br m, 12H; PCH_2CH_2), 1.65–1.45 (br m, 12H; $PCH_2CH_2CH_2$), 1.37–1.11 ppm (br m, remaining CH_2); $^{13}C\{^1H\}$ NMR: $\delta = 30.1$ (virtual t,[23] $^3J_{CP} = 6.8$ Hz, $PCH_2CH_2CH_2$), 28.1 (s, CH_2), 27.2 (s, CH_2), 27.1 (s, CH_2), 26.8 (s, CH_2), 24.1 (virtual t,[23] $^1J_{CP} = 13.7$ Hz, PCH_2), 23.7 (s, CH_2); $^{31}P\{^1H\}$ 10.6 ppm (s); IR (powder film): $\tilde{\nu} = 2921$ (s), 2852 (s), 1636 (m), 1457 (m), 1410 (w), 1262 (m), 1104 (m), 1015 (m), 800 (m), 715 cm^{-1} (m); MS:[49a] *m/z* (%): 916 (40) $[M]^+$, 837 (100) $[M-Br]^+$, 755 (85) $[M-2Br]^+$.

***trans*-[$\overline{PdI_2(P\{(CH_2)_{14}\}_3P)}$] (*trans*-10c)**: A 5 mm NMR tube was sequentially charged with *trans*-**5c** (0.0164 g, 0.0198 mmol), NaI (0.0119 g, 0.0793 mmol) and THF/acetone (0.7 mL; 1:1 v/v). After 10 min, a $^{31}P\{^1H\}$ NMR spectrum showed >99% conversion. The solvent was removed by oil pump vacuum. The residue was extracted with benzene. The solvent was removed from the extract by freeze pump drying to give *trans*-**10c** as an orange powder (0.0184 g, 0.0182 mmol, 92%).

M.p. (capillary) 124–125 °C; DSC ($T_i/T_e/T_p/T_f$): 79.1/105.4/115.3/116.3 °C (endotherm), 116.2/119.8/127.9/131.5 °C (endotherm); TGA: onset of mass loss, 226 °C; elemental analysis calcd (%) for $C_{42}H_{84}I_2P_2Pd$: C 49.88, H 8.37; found: C 50.23, H 8.55; ^1H NMR ($CDCl_3$):[51] $\delta = 2.24$–2.12 (br m, 12H; PCH_2), 1.60–1.48 (br m, 12H; PCH_2CH_2), 1.48–1.38 (br m, 12H; $PCH_2CH_2CH_2$), 1.38–1.20 ppm (br m, remaining CH_2); $^{13}C\{^1H\}$ NMR: $\delta = 30.0$ (virtual t,[23] $^3J_{CP} = 6.8$ Hz, $PCH_2CH_2CH_2$), 28.2 (partially obscured virtual t,[23] $^1J_{CP} = 13.7$ Hz, PCH_2), 28.1 (s, CH_2), 27.2 (s, CH_2), 27.1 (s, CH_2), 26.8 (s, CH_2), 24.1 ppm (s, PCH_2); $^{31}P\{^1H\}$ NMR: $\delta = 4.4$ ppm (s); IR (powder film): $\tilde{\nu} = 2921$ (s), 2852 (s), 1461 (m), 1441 (m), 1414 (m), 1351 (m), 1158 (m), 1088 (s), 1013 (m), 775 (m), 721 (m), 710 cm^{-1} (m); MS:[49a] *m/z* (%): 883 (100) $[M-I]^+$, 756 (40) $[M-2I]^+$.

***trans*-[$\overline{PtBr_2(P\{(CH_2)_{14}\}_3P)}$] (*trans*-7c)**: A 5 mm NMR tube was sequentially charged with *trans*-**4c** (0.0181 g, 0.0197 mmol), LiBr (0.0068 g, 0.079 mmol), and THF (0.6 mL). After 27 h, a $^{31}P\{^1H\}$ NMR spectrum showed >99% conversion. The solvent was removed by oil pump vacuum, and benzene was added. The suspension was filtered through a glass fiber filter. The solvent was removed from the filtrate by freeze pump drying to give *trans*-**7c** as a yellow powder (0.0148 g, 0.0147 mmol, 75%).

M.p. (capillary) 119–121 °C; DSC ($T_i/T_e/T_p/T_c/T_f$): 88.1/121.4/124.0/125.9/140.4 °C (endotherm); TGA: onset of mass loss, 283 °C; elemental analysis calcd (%) for $C_{42}H_{84}Br_2P_2Pt$: C 50.15, H 8.42; found: C 50.20, H 8.63; ^1H NMR ($CDCl_3$):[51] $\delta = 1.94$–1.89 (br m, 12H; PCH_2), 1.62–1.59 (br m, 12H; PCH_2CH_2), 1.44–1.39 (br m, 12H; $PCH_2CH_2CH_2$), 1.38–1.29 ppm (br m, remaining CH_2); $^{13}C\{^1H\}$ NMR: 29.9 (virtual t,[23] $^3J_{CP} = 6.8$ Hz, $PCH_2CH_2CH_2$), 28.1 (s, CH_2), 27.2 (s, CH_2), 27.1 (s, CH_2), 26.8 (s, CH_2), 23.2 (s, PCH_2CH_2), 22.7 ppm (virtual t,[23] $^1J_{CP} = 16.7$ Hz, PCH_2); $^{31}P\{^1H\}$ NMR: 2.8 ppm (s, $^1J_{PPt} = 2344$ Hz);[48] IR (powder film): $\tilde{\nu} = 2921$ (s), 2852 (s), 1455 (m), 1412 (m), 1403 (m), 1351 (m), 1262 (m), 1092 (m), 1065 (m), 1052 (m), 1015 (m), 793 (m), 716 cm^{-1} (m); MS:[49a] *m/z* (%): 1006 (10) $[M]^+$, 926 (55) $[M-Br]^+$, 845 (100) $[M-2Br]^+$.

***trans*-[$\overline{PtI_2(P\{(CH_2)_{14}\}_3P)}$] (*trans*-9c)**: Complex *trans*-**4c** (0.0159 g, 0.0173 mmol), NaI (0.0104 g, 0.0694 mmol) and THF/acetone (0.6 mL, 1:1 v/v) were combined as in the procedure for *trans*-**7c**. After 24 h, an identical workup gave *trans*-**9c** as an orange powder (0.0110 g, 0.0100 mmol, 58%).

M.p. (capillary) 122–123 °C; DSC ($T_i/T_e/T_p/T_c/T_f$): 98.7/117.5/120.2/121.6/121.6 °C (endotherm), 124.7/125.5/128.6/130.4/133.6 °C (endotherm); TGA: onset of mass loss, 286 °C; elemental analysis calcd (%) for $C_{42}H_{84}I_2P_2Pt$: C 45.86, H 7.70; found: C 45.76, H 7.63; ^1H NMR ($CDCl_3$):[51] $\delta = 2.21$–2.17 (br m, 12H; PCH_2), 1.54–1.41 (br m, 12H; PCH_2CH_2), 1.43–1.38 (br m, 12H; $PCH_2CH_2CH_2$), 1.38–1.13 ppm (br m, remaining CH_2); $^{13}C\{^1H\}$ NMR: $\delta = 29.8$ (virtual t,[23] $^3J_{CP} = 6.5$ Hz, $PCH_2CH_2CH_2$), 28.1 (s, CH_2), 27.2 (s, CH_2), 27.1 (s, CH_2), 26.7 (s, CH_2), 26.3 (virtual t,[23] $^1J_{CP} = 17.5$ Hz, PCH_2), 23.5 ppm (s, PCH_2CH_2); $^{31}P\{^1H\}$ NMR: $\delta = -3.6$ ppm (s, $^1J_{PPt} = 2283$ Hz);[48] IR (powder film): $\tilde{\nu} = 2921$ (s), 2852 (s), 1461 (m), 1441 (m), 1204 (m), 1158 (m), 1015 (m), 965 (m), 778 (m), 722 (m), 677 cm^{-1} (m); MS:[49a] *m/z* (%): 972 (100) $[M-I]^+$.

***trans*-[$\overline{PdBr_2(P\{(CH_2)_{18}\}_3P)}$] (*trans*-8e)**: Complex *trans*-**5c** (0.0173 g, 0.0174 mmol). THF (0.6 mL) and LiBr (0.0046 g, 0.053 mmol) were combined as in procedure B for *trans*-**8c**. A similar workup (extract filtered through a glass fiber filter) gave *trans*-**8e** as a yellow powder (0.0132 g, 0.0122 mmol, 70%).

DSC ($T_i/T_e/T_p/T_f$): 37.1/39.9/51.1/56.3 °C (endotherm); TGA: onset of mass loss, 233 °C; elemental analysis calcd (%) for $C_{54}H_{108}Br_2P_2Pd$: C 59.74, H 10.03; found: C 59.19, H 9.29;[50] ^1H NMR ($CDCl_3$):[51] $\delta =$ 1.99–1.90 (br m, 12H; PCH_2), 1.60–1.48 (br m, 12H; PCH_2CH_2), 1.48–1.35 (br m, 12H; $PCH_2CH_2CH_2$), 1.35–1.15 ppm (br m, remaining CH_2); $^{13}C\{^1H\}$ NMR: $\delta = 30.7$ (virtual t,[23] $^3J_{CP} = 6.5$ Hz, $PCH_2CH_2CH_2$), 28.5 (s, CH_2), 28.3 (s, CH_2), 28.2 (s, $2CH_2$), 27.9 (s, CH_2), 27.6 (s, CH_2), 24.0 (s, PCH_2CH_2), 23.5 ppm (virtual t,[23] $^1J_{CP} = 13.6$ Hz, PCH_2); $^{31}P\{^1H\}$ NMR: $\delta = 7.9$ ppm (s); IR (powder film): $\tilde{\nu} = 2921$ (s), 2851 (s), 1460 (m), 1416 (m), 1350 (m), 1262 (m), 1097 (m), 1058 (s), 1036 (m), 795 (m), 719 cm^{-1} (m).

***trans*-[$\overline{PdI_2(P\{(CH_2)_{18}\}_3P)}$] (*trans*-10e)**: Complex *trans*-**5c** (0.0159 g, 0.0160 mmol), NaI (0.0096 g, 0.064 mmol) and THF/acetone (0.6 mL; 1:1 v/v) were combined as in the procedure for *trans*-**7c**. After 10 min, an identical workup gave *trans*-**10e** as an orange powder (0.0154 g, 0.0131 mmol, 82%).

M.p. (capillary) 26–30 °C; DSC ($T_i/T_e/T_p/T_c/T_f$): 29.8/29.8/39.3/44.9/48.6 °C (endotherm); TGA: onset of mass loss, 184 °C; elemental analysis calcd (%) for $C_{54}H_{108}I_2P_2Pd$: C 53.52, H 8.53; found: C 54.64, H 9.24;[50] ^1H NMR ($CDCl_3$):[51] $\delta = 2.30$–2.20 (br m, 12H; PCH_2), 1.56–1.48 (br m, 12H; PCH_2CH_2), 1.48–1.36 (br m, 12H; $PCH_2CH_2CH_2$), 1.36–1.25 ppm (br m, remaining CH_2); $^{13}C\{^1H\}$ NMR: $\delta = 31.0$ (virtual t,[23] $^3J_{CP} = 6.6$ Hz, $PCH_2CH_2CH_2$), 28.9 (s, CH_2), 28.7 (s, CH_2), 28.6 (s, $2CH_2$), 28.35 (virtual t,[23] partially obscured by other signal, $^1J_{CP} =$ 17.1 Hz, PCH_2), 28.29 (s, CH_2), 28.0 (s, CH_2), 24.8 ppm (s, PCH_2CH_2); $^{31}P\{^1H\}$ NMR: $\delta = 1.5$ ppm (s); MS:[49a] *m/z* (%): 1051 (80) $[M-I]^+$.

***trans*-[$\overline{Pt(CN)_2(P\{(CH_2)_{14}\}_3P)}$] (*trans*-11c)**: A 5 mL vial was sequentially charged with *trans*-**4c** (0.0231 g, 0.0252 mmol), KCN (0.0033 g, 0.051 mmol), and CH_2Cl_2/CH_3OH (2.0 mL, 1:2 v/v). After 16 h, a $^{31}P\{^1H\}$ NMR spectrum showed >99% conversion. The sol-

vent was removed by oil pump vacuum, and benzene was added. The suspension was filtered through a glass fiber filter. The solvent was removed from the filtrate by freeze pump drying to give *trans*-**11c** as a white powder (0.0205 g, 0.0228 mmol, 90%). M.p. (capillary) 171–172 °C; DSC ($T_i/T_e/T_p/T_c/T_f$): 111.1/125.3/128.1/133.4/133.9 °C (endotherm), 151.0/153.4/159.1/163.8/164.3 °C (endotherm), 164.4/170.0/174.3/176.5/180.1 °C (endotherm); TGA: onset of mass loss, 244 °C; elemental analysis calcd (%) for $C_{44}H_{84}N_2P_2Pt$: C 58.84, H 9.43, N 3.12; found: C 58.61, H 9.53, N 3.02; ^{1}H NMR ($CDCl_3$):[51] δ = 2.30–2.03 (br m, 12H; PCH_2), 1.62–1.58 (br m, 12H; PCH$_2$CH_2), 1.52–1.46 (br m, 12H; PCH$_2$CH$_2$CH_2), 1.42–1.22 ppm (br m, remaining CH_2); ^{13}C{^{1}H} NMR: 124.3 (t, $^2J_{CP}$ = 17.2 Hz, *C*N), 29.8 (virtual t,[23] $^3J_{CP}$ = 7.0 Hz, PCH$_2$CH$_2$CH_2), 27.9 (s, CH_2), 27.2 (s, CH_2), 27.0 (s, CH_2), 26.7 (s, CH_2), 24.9 (virtual t,[23] $^1J_{CP}$ = 17.2 Hz, PCH_2), 23.7 ppm (s, PCH$_2$CH_2); ^{31}P{^{1}H} NMR: δ = 9.2 ppm (s, $^1J_{PPt}$ = 2166 Hz);[48] IR (powder film): $\tilde{\nu}$ = 2919 (s), 2850 (s), 2124 (m, ν_{CN}), 1465 (m), 1447 (m), 1414 (m), 1262 (w), 1106 (m), 1004 (m), 801 (m), 721 (m), 708 (m); MS:[49a] *m/z* (%): 898 (70) $[M]^+$, 683 (80) $[OP\{(CH_2)_{14}\}_3PO]^+$, 667 (100) $[P\{(CH_2)_{14}\}_3PO]^+$, 651 (20) $[P\{(CH_2)_{14}\}_3P]^+$.

***trans*-[Pd(CN)$_2$(P{(CH$_2$)$_{14}$}$_3$P)] (*trans*-12c).** Complex *trans*-**5c** (0.0605 g, 0.0730 mmol), KCN (0.0190 g, 0.292 mmol), and CH_2Cl_2/CH_3OH (3.0 mL, 1:2 v/v) were combined as in the procedure for *trans*-**11c**. After 10 min, an identical workup gave *trans*-**12c** as a white powder (0.0509 g, 0.0629 mmol, 86%).

M.p. (capillary) 183–187 °C; DSC ($T_i/T_e/T_p/T_c/T_f$): 39.1/56.1/64.0/68.3/77.0 °C (endotherm), 196.6/197.9/211.2/217.4./219.7 °C (endotherm); TGA: onset of mass loss, 260 °C; elemental analysis calcd (%) for $C_{44}H_{84}N_2P_2Pd$: C 65.28, H 10.46, N 3.46; found: C 66.65, H 10.26, N 3.04;[50] ^{1}H NMR ($CDCl_3$):[51] δ = 1.96–1.94 (br m, 12H; PCH_2), 1.58–1.53 (br m, 12H; PCH$_2$CH_2), 1.46–1.41 (br m, 12H; PCH$_2$CH$_2$CH_2), 1.35–1.15 ppm (br m, remaining CH_2); ^{13}C{^{1}H} NMR: δ = 129.5 (t, $^2J_{CP}$ = 14.1 Hz, *C*N), 30.0 (virtual t,[23] $^3J_{CP}$ = 7.0 Hz, PCH$_2$CH$_2$CH_2), 27.9 (s, CH_2), 27.2 (s, CH_2), 26.9 (s, CH_2), 26.8 (s, CH_2), 25.7 (virtual t,[23] $^1J_{CP}$ = 14.3 Hz, PCH_2), 24.0 ppm (s, PCH$_2$CH$_2$); ^{31}P{^{1}H} NMR: δ = 17.4 ppm (s); IR (powder film): $\tilde{\nu}$ = 2919 (s), 2850 (s), 2142 (s, ν_{CN}), 1465 (m), 1414 (m), 1106 (m), 1025 (w), 801 (m), 721 (m), 708 ppm (m); MS:[49a] *m/z* (%): 809 (50) $[M]^+$, 683 (100) $[OP\{(CH_2)_{14}\}_3PO]^+$, 667 (55) $[P\{(CH_2)_{14}\}_3PO]^+$, 651 (25) $[P\{(CH_2)_{14}\}_3P]^+$.

***trans*-[Pt(CN)$_2$(P{(CH$_2$)$_{18}$}$_3$P)] (*trans*-11e)**: Complex *trans*-**4e** (0.0301 g, 0.0277 mmol), KCN (0.0038 g, 0.0584 mmol) and CH_2Cl_2/CH_3OH (1:2 v/v) were combined as in the procedure for *trans*-**11c**. After 18 h, an identical workup gave *trans*-**11e** as a white powder (0.0269 g, 0.0252 mmol, 91%).

DSC ($T_i/T_e/T_p/T_c/T_f$): 109.2/151.0/168.1/178.3/173.2 °C (endotherm); TGA: onset of mass loss, 286 °C; elemental analysis calcd (%) for $C_{56}H_{108}N_2P_2Pt$: C 63.07, H 10.21, N 2.63; found: C 64.18, H 10.45, N 2.25;[50] ^{1}H NMR ($CDCl_3$):[51] δ = 2.59–1.92 (br m, 12H; PCH_2), 1.68–1.52 (br m, 12H; PCH$_2$CH_2), 1.52–1.36 (br m, 12H; PCH$_2$CH$_2$CH_2), 1.36–1.16 ppm (br m, remaining CH_2); ^{13}C{^{1}H} NMR: δ = 124.7 (virtual t,[23] $^2J_{CP}$ = 17.2 Hz, *C*N), 30.5 (virtual t,[23] $^3J_{CP}$ = 6.9 Hz, PCH$_2$CH$_2$CH_2), 28.5 (s, CH_2), 28.4 (s, CH_2), 28.3 (s, CH_2), 28.1 (s, CH_2), 27.8 (s, CH_2), 27.5 (s, CH_2), 24.7 (virtual t,[23] $^1J_{CP}$ = 17.3 Hz, PCH_2), 24.1 ppm (s, PCH$_2$CH$_2$); ^{31}P{^{1}H} NMR: δ = 6.8 ppm (s, $^1J_{PPt}$ = 2152 Hz);[48] IR (powder film): $\tilde{\nu}$ = 2918 (s), 2849 (s), 2123 (w, ν_{CN}), 1471 (m), 1417 (w), 1108 (w), 1124 (w), 799 (w), 749 (m), 722 (m); MS:[49a] *m/z* (%): 1066 (100) $[M]^+$.

***trans*-[Pt(NCS)$_2$(P{(CH$_2$)$_{14}$}$_3$P)] (*trans*-13c) and *trans*-[Pt(NCS)(SCN)(P{(CH$_2$)$_{14}$}$_3$P)] (*trans*-14c)**: A 5 mL vial was sequentially charged with *trans*-**4c** (0.0656 g, 0.0715 mmol), KSCN (0.0286 g, 0.294 mmol), and THF/acetone (3.0 mL, 1:1 v/v). After 5 h, the mixture was filtered. The solvent was removed from the filtrate by rotary evaporation. The sample was partially dissolved in THF/CH_2Cl_2 (2:1 v/v) and subjected to chromatography on a silica column (2×30 cm, 1:1 v/v CH_2Cl_2/hexanes). The solvents were removed from the product fractions by rotary evaporation to give *trans*-**14c** (0.0140 g, 0.0145 mmol, 20%; R_f = 0.57) and *trans*-**13c** (0.0190 g, 0.0197 mmol, 28%; R_f = 0.40) as white crystalline solids.

Data for trans-***13c***: M.p. (capillary) 210–212 °C; DSC ($T_i/T_e/T_p/T_c/T_f$): 179.5/189.6/199.0/205.6/202.6 °C (endotherm), 205.3/210.1/213.8/215.6/219.7 °C (endotherm); TGA: onset of mass loss, 270 °C; elemental analysis calcd (%) for $C_{44}H_{84}N_2P_2PtS_2$: C 54.92, H 8.80, N 2.91, S 6.66; found: C 55.04, H 8.84, N 2.68, S 6.21; ^{1}H NMR ($CDCl_3$):[51] δ = 1.95–1.86 (br m, 12H; PCH_2), 1.68–1.46 (br m, 24H; PCH_2CH_2), 1.43–1.25 ppm (br m, remaining CH_2); ^{13}C{^{1}H}[29] NMR: δ = 30.2 (virtual t,[23] J_{CP} = 6.8 Hz, 2PCH$_2$CH$_2$CH$_2$), 29.4 (virtual t,[23] J_{CP} = 6.5 Hz, PCH$_2$CH$_2$CH$_2$), 28.4 (s, CH_2), 27.9 (s, CH_2), 27.8 (s, CH_2), 27.3 (s, CH_2), 26.8 (s, CH_2), 26.7 (s, 2CH_2), 26.6 (s, CH_2), 23.7 (s, CH_2), 22.4 (s, CH_2), 20.0 ppm (s, CH_2); ^{31}P{^{1}H} NMR: δ = 11.3 ppm (s, $^1J_{PPt}$ = 2258 Hz);[48] IR (powder film): $\tilde{\nu}$ = 2925 (s), 2852 (s), 2111 (s, ν_{NCS}), 1461 (m), 1441 (m), 1414 (m), 1260 (w), 1094 (m), 1042 (m), 1015 (w), 853 (m), 797 (m), 722 (m); MS:[49a] *m/z* (%): 962 (100) $[M]^+$, 904 (35) $[M-SCN]^+$.

Data for trans-***14c***: M.p. (capillary) 211–213 °C; DSC ($T_i/T_e/T_p/T_c/T_f$): 182.8/210.6/217.6/222.2/229.0 °C (endotherm); TGA: onset of mass loss, 283 °C; elemental analysis calcd (%) for $C_{44}H_{84}N_2P_2PtS_2$: C 54.92, H 8.80, N 2.91, S 6.66; found: C 54.95, H 8.59, N 2.75, S 6.20; ^{1}H NMR ($CDCl_3$): δ = 2.17–1.97 (br m, 6H; CH_2), 1.86–1.69 (br m, 14H; CH_2), 1.69–1.60 (br m, 2H; CH_2), 1.59–1.47 (br m, 20H; CH_2), 1.47–1.39 (br m, 8H; CH_2), 1.39–1.17 ppm (br m, 34H; CH_2); ^{13}C{^{1}H}[29] NMR: δ = 30.8 (virtual t,[23] J_{CP} = 7.0 Hz, PCH$_2$CH$_2$CH$_2$), 29.5 (virtual t,[23] J_{CP} = 6.5 Hz, 2PCH$_2$CH$_2$CH$_2$), 28.4 (s, 2CH_2), 28.0 (s, CH_2), 27.7 (s, 2CH_2), 27.2 (s, CH_2), 26.83 (s, 2CH_2), 26.78 (s, CH_2), 26.6 (s, CH_2), 25.7 (s, CH_2), 25.1 (s, CH_2), 22.2 (s, CH_2), 20.9 ppm (virtual t,[23] $^1J_{CP}$ = 16.2 Hz, PCH$_2$); ^{31}P{^{1}H} NMR: δ = 13.4 ppm (s, $^1J_{PPt}$ = 2224 Hz);[48] IR (powder film): $\tilde{\nu}$ = 2921 (s), 2848 (s), 2107 (s, ν_{NCS}), 2005 (m, ν_{SCN}), 1457 (m), 1441 (m), 1260 (m), 1260 (w), 1092 (s), 1021 (s), 795 (s), 717 cm^{-1} (m); MS:[49a] *m/z* (%): 962 (95) $[M]^+$, 904 (100) $[M-SCN]^+$.

***trans*-[PtPh$_2$(P{(CH$_2$)$_{14}$}$_3$P)] (*trans*-15c).** A Schlenk flask was charged with *trans*-**4c** (0.1004 g, 0.1095 mmol) and Ph_2Zn (0.0718 g, 0.327 mmol), and THF (3.5 mL) was added with stirring. After 20 h, a few drops of CH_3OH were added. The sample was exposed to air. After 1 h, the solvent was removed by trap to trap distillation, and benzene was added. The suspension was filtered through a pipette packed with silica gel. The pipette was rinsed with benzene. The solvent was removed from the filtrate by freeze pump drying to give *trans*-**15c** as a white powder (0.0663 g, 0.0663 mmol, 61%).

M.p. (capillary) 178–179 °C (slight discolorization, 101 °C); DSC ($T_i/T_e/T_p/T_c/T_f$): 68.3/78.5/89.2/102.3/110.0 °C (endotherm), 173.4/186.4/188.9/190.8/196.6 °C (endotherm); TGA: onset of mass loss, 312 °C; elemental analysis calcd (%) for $C_{54}H_{94}P_2Pt$: C 64.84, H 9.47; found: C 65.37, H 9.58; ^{1}H NMR ($CDCl_3$):[53] δ = 7.49 (d, $^1J_{HH}$ = 7.2 Hz, 2H; *o*-Ph), 7.38 (d, $^1J_{HH}$ = 7.0 Hz, 2H; *o*′-Ph), 7.02 (apparent t, $^1J_{HH}$ = 7.2 Hz, 2H; *m*-Ph), 6.95 (apparent t, $^1J_{HH}$ = 7.2 Hz, 2H; *m*′-Ph), 6.79 (apparent t, $^1J_{HH}$ = 7.2 Hz, 2H; *p*-Ph), 1.94–1.74 (br m, 6H; CH_2), 1.70–1.55 (br m, 6H; CH_2), 1.55–1.30 (br m, 50H; CH_2), 1.30–1.12 ppm (br m, 22H; CH_2); ^{13}C{^{1}H} NMR: δ = 162.0 (s, $^2J_{CPt}$ = 10.8 Hz, *i*-Ph), 141.4 (s, *o*-Ph), 139.2 (s, *o*′-Ph), 126.7 (s, $^4J_{CPt}$ = 21.2 Hz, *m*-Ph),[48] 126.0 (s, *m*′-Ph), 120.7 (s, *p*-Ph), 30.6 (virtual t,[23] J_{CP} = 6.9 Hz, CH_2), 29.0 (s, 2CH_2), 28.8 (s, 2CH_2), 28.7 (partially obscured virtual t,[23] J_{CP} = 6.6 Hz, PCH$_2$CH$_2$CH$_2$), 28.3 (s, CH_2), 27.6 (s, CH_2), 27.1 (s, CH_2), 26.8 (s, CH_2), 26.6 (s, 2CH_2), 26.4 (s, 2CH_2), 26.0 (s, CH_2), 25.1 (s, CH_2), 22.3 (virtual t,[23] J_{CP} = 15.7 Hz, PCH$_2$), 21.4 ppm (virtual t,[23] J_{CP} = 16.8 Hz, PCH$_2$); ^{31}P{^{1}H} NMR: δ = 3.0 ppm (s, $^1J_{PPt}$ = 2837 Hz);[48] IR (powder

film): $\tilde{\nu}$ = 3019 (w), 2922 (m), 1174 (s), 1440 (w), 1366 (s), 1216 (s), 1029 (w), 1019 (w), 799 cm^{-1} (w); MS:[49a] *m/z* (%): 1000 (10) $[M]^+$, 923 (100) $[M-Ph]^+$.

***trans*-[$\overbrace{PtPh_2(P\{(CH_2)_{18}\}_3P)}$] (*trans*-15 e)**: Complex *trans*-**4 e** (0.0431 g, 0.0397 mmol), Ph_2Zn (0.0261 g, 0.1189 mmol), and THF (4 mL), and CH_3OH (0.1 mL) were combined as in the procedure for *trans*-**15 c**. An identical workup gave a white powder. Crystallization from CH_2Cl_2/pentane gave *trans*-**15 e** as colorless needles (0.0417 g, 0.0357 mmol, 90%).

DSC ($T_i/T_e/T_p/T_c/T_f$): 116.8/140.9/144.7/146.3/164.3 °C (endotherm); TGA: onset of mass loss, 234 °C; elemental analysis calcd (%) for $C_{66}H_{118}P_2Pt$: C 67.83, H 10.18; found: C 66.66, H 10.43;[50] ^{1}H NMR ($CDCl_3$):[51] δ = 7.38 (d, $^1J_{HH}$ = 7.2 Hz, 4H; *o*-Ph), 6.95 (apparent t, $^1J_{HH}$ = 7.2 Hz, 4H; *m*-Ph), 6.77 (apparent t, $^1J_{HH}$ = 7.2 Hz, 2H; *p*-Ph), 1.45–1.42 (br m, 12H; PCH_2), 1.36–1.28 (br m, 42H; PCH_2CH_2), 1.24–1.05 ppm (br m, 54H; CH_2); $^{13}C\{^1H\}$[54] NMR: δ = 140.5 (s, *o*-Ph), 127.2 (s, *m*-Ph), 121.1 (s, *p*-Ph), 30.3 (virtual t,[23] $^3J_{CP}$ = 7.0 Hz, $PCH_2CH_2CH_2$), 28.7 (s, CH_2), 28.7 (s, $2CH_2$), 28.4 (s, CH_2), 28.1 (s, CH_2), 28.0 (s, CH_2), 27.8 (s, PCH_2CH_2), 21.6 ppm (virtual t,[23] $^1J_{CP}$ = 17.3 Hz, PCH_2); $^{31}P\{^1H\}$ NMR: δ = 3.2 ppm (s, $^1J_{PPt}$ = 2807 Hz);[48] IR (powder film): $\tilde{\nu}$ = 2922 (s), 2853 (s), 1567 (w), 1459 (m), 1262 (m), 1092 (m), 1023 (m), 799 (s), 734 cm^{-1} (s); MS:[49a] *m/z* (%): 1090 (85) $[M-Ph]^+$.

$P\{(CH_2)_{14}\}_3P$ (18). A Schlenk flask was charged with NaC≡CH (1.368 g, 28.49 mmol) and THF (30 mL). A solution of *trans*-**4 c** (0.523 g, 0.570 mmol) in THF (20 mL) was added to the suspension with stirring. After 3 d, the mixture was filtered. The filter cake was washed with THF (3×5 mL). The solvent was removed from the filtrate by oil pump vacuum. Hexanes (50 mL) were added to the solid residue. The suspension was filtered through celite and the filter cake was washed with hexanes (3×5 mL). The solvents were removed from the filtrate and the solid residue dried (15 h) by oil pump vacuum to give **18** as a white powder (0.339 g, 0.521 mmol, 91%). M.p. 68 °C; elemental analysis calcd (%) for $C_{42}H_{84}P_2$: C 77.48, H 13.00; found: C 77.67, H 13.08; ^{1}H NMR ($CDCl_3$): δ = 1.37–1.32, 1.31–1.23 ppm (2 br m, 84H; CH_2); $^{13}C\{^1H\}$ NMR: δ = 31.2 (d, J_{CP} = 10.3 Hz, CH_2), 29.2 (s, CH_2), 29.14 (s, CH_2), 29.08 (s, CH_2), 28.7 (s, CH_2), 26.3 (d, J_{CP} = 12.2 Hz, CH_2), 25.2 ppm (d, J_{CP} = 11.0 Hz, CH_2); $^{31}P\{^1H\}$ NMR: δ = −30.1 ppm (s); MS:[49b] *m/z* (%): 651.6 (58) $[M+H]^+$.

$\overbrace{(CH_2)_{14}}P(CH_2)_{14}P\overbrace{(CH_2)_{14}}$ (19). A Schlenk flask was charged with NaC≡CH (0.399 g, 8.309 mmol) and THF (10 mL). A solution of *trans*-**4′e** (0.153 g, 0.167 mmol) in THF (10 mL) was added to the suspension with stirring. After 9 d, the mixture was filtered through celite. The filter cake was washed with THF (6×5 mL). The solvent was removed from the filtrate and the residue dried (10 h) by oil pump vacuum. Hexanes (20 mL) were added. The suspension was filtered through celite and the filter cake was washed with hexanes (6×5 mL). The solvents were removed from the filtrate and the residue dried (24 h) by oil pump vacuum to give **19** as a white powder (0.098 g, 0.151 mmol, 90%).

M.p. 74 °C; elemental analysis calcd (%) for $C_{42}H_{84}P_2$: C 77.48, H 13.00; found: C 75.94, H 12.90;[50] ^{1}H NMR ($CDCl_3$): δ = 1.46–1.41, 1.37–1.31, 1.28–1.26, 1.23 ppm (3 br m, 1 apparent s, 84H; CH_2); $^{13}C\{^1H\}$ NMR: δ = 31.5 (d, J_{CP} = 11.2 Hz, CH_2), 29.66 (s, $2CH_2$), 29.56 (s, CH_2), 29.42 (s, CH_2), 29.16 (d, J_{CP} = 9.8 Hz, $2CH_2$), 27.8 (d, J_{CP} = 9.8 Hz, CH_2), 27.15 (d, J_{CP} = 13.1 Hz, $2CH_2$), 27.08 (s, $2CH_2$), 26.8 (s, $2CH_2$), 26.6 (s, $2CH_2$), 26.19 (s, $2CH_2$), 26.16 (d, J_{CP} = 13.8 Hz, CH_2), 24.7 ppm (d, J_{CP} = 12.0 Hz, $2CH_2$); $^{31}P\{^1H\}$ NMR: δ = −30.9 ppm (s); MS:[49b] *m/z* (%): 651.6 (12) $[M+H]^+$, 326.3 (100) $[M+2H]^{2+}$; HRMS (ESI+): *m/z* calcd for $C_{42}H_{85}P_2$ $[M+H]^+$: 651.6127; found: 651.6533.

$H_3B(\overbrace{CH_2)_{14}}P(C_{14}H_{28})P\overbrace{(CH_2)_{14}}BH_3$ (19·2 BH_3). A Schenk flask was charged with *trans*-**4′e** (0.029 g, 0.032 mmol), NaC≡CH (0.042 g, 18 wt% in xylene, 0.157 mmol), and THF (1 mL) with stirring. After 72 h, the solvent was removed by oil pump vacuum. The residue was placed on a plug of silica gel in a Pasteur pipette and rinsed with benzene. The solvent was removed from the filtrate, and THF (1 mL) and $BH_3{\cdot}S(CH_3)_2$ (0.10 mL, 2.0 M in THF, 0.20 mmol) were added. After 15 min, the solvent was removed by oil pump vacuum. The residue was placed on a plug of silica gel in a Pasteur pipette and rinsed with hexanes/CH_2Cl_2 (2:1 v/v). The solvent was removed by oil pump vacuum to give **19**·2 BH_3 (0.017 g, 0.025 mmol, 78%) as a white solid. The NMR data closely corresponded to those obtained with an independently prepared sample that was additionally characterized by microanalysis and mass spectrometry.[30]

Crystallography: Details of the crystallographic investigation can be found in the Supporting Information. CCDC 956025 (*trans*-**4 c**), 608961 (*trans*-**5 c**), 956148 (*trans*-**7 c**), 956019 (*trans*-**8 c**), 956020 (*trans*-**9 c**), 956024 (*trans*-**10 c**), 956021 (*trans*-**13 c**), 608960 (*trans*-**15 c**·*n*-C_5H_{12}), 955782 (*trans*-**15 e**) and 956018 (**15 c**·2 BH_3) contain the supplementary crystallographic data for this paper. These data can be obtained free of charge from The Cambridge Crystallographic Data Centre via www.ccdc.cam.ac.uk/data_request/cif.

Acknowledgements

We thank the US National Science Foundation (CHE-0719267 and CHE-1153085), the Deutsche Forschungsgemeinschaft (DFG, GL 300/9-1), and Johnson Matthey PMC (precious metal loans) for support, and Dr. Tobias Fiedler for some helpful calculations.

Keywords: diphosphine ligands · hydrogenation · olefin metathesis · palladium · platinum · substitution reactions

[1] See http://www.gyroscopes.org/uses.asp. The authors are unaware of any books or peer reviewed articles that match the diversity of examples on the gyroscope.org web site, which is maintained by G. Turner.
[2] R. M. Alexander, *Science* **2007**, *315*, 771.
[3] a) E. Butikov, *Eur. J. Phys.* **2006**, *27*, 1071; b) D. Kleppner, R. J. Kolenkow, *An Introduction to Mechanics*, Cambridge University Press, Cambridge, **2010**, Chapters 7.3–7.5.
[4] G. S. Kottas, L. I. Clarke, D. Horinek, J. Michl, *Chem. Rev.* **2005**, *105*, 1281.
[5] a) K. Liu, W. Zhang, W. Chen, K. Li, F. Dai, F. Cui, X. Wu, G. Ma, Q. Xiao, *J. Micromech. Microeng.* **2009**, *19*, 113001; b) M. N. Armenise, C. Ciminelli, F. Dell'Olio, V. M. N. Passaro, *Advances in Gyroscope Technologies*, Springer, Heidelberg, **2011**.
[6] T. Shima, F. Hampel, J. A. Gladysz, *Angew. Chem.* **2004**, *116*, 5653; *Angew. Chem. Int. Ed.* **2004**, *43*, 5537.
[7] A. J. Nawara, T. Shima, F. Hampel, J. A. Gladysz, *J. Am. Chem. Soc.* **2006**, *128*, 4962.
[8] L. Wang, F. Hampel, J. A. Gladysz, *Angew. Chem.* **2006**, *118*, 4479; *Angew. Chem. Int. Ed.* **2006**, *45*, 4372.
[9] L. Wang, T. Shima, F. Hampel, J. A. Gladysz, *Chem. Commun.* **2006**, 4075.
[10] G. D. Hess, F. Hampel, J. A. Gladysz, *Organometallics* **2007**, *26*, 5129.
[11] See also a) K. Skopek, M. Barbasiewicz, F. Hampel, J. A. Gladysz, *Inorg. Chem.* **2008**, *47*, 3474; b) J. Han, C. Deng, L. Wang, J. A. Gladysz, *Organometallics* **2010**, *29*, 3231.
[12] K. Skopek, J. A. Gladysz, *J. Organomet. Chem.* **2008**, *693*, 857.
[13] P. D. Zeits, G. P. Rachiero, F. Hampel, J. H. Reibenspies, J. A. Gladysz, *Organometallics* **2012**, *31*, 2854.
[14] a) T.-A. V. Khuong, J. E. Nuñez, C. E. Godinez, M. A. Garcia-Garibay, *Acc. Chem. Res.* **2006**, *39*, 413; b) C. S. Vogelsberg, M. A. Garcia-Garibay, *Chem. Soc. Rev.* **2012**, *41*, 1892.
[15] Additional literature subsequent to reference [14a] or [14b]: a) J. E. Nuñez, A. Natarajan, S. I. Khan, M. A. Garcia-Garibay, *Org. Lett.* **2007**, *9*,

3559; b) P. Commins, J. E. Nuñez, M. A. Garcia-Garibay, *J. Org. Chem.* **2011**, *76*, 8355; c) B. Rodríguez-Molina, S. Pérez-Estrada, M. A. Garcia-Garibay, *J. Am. Chem. Soc.* **2013**, *135*, 10388; d) M. Hughs, M. Jimenez, S. Khan, M. A. Garcia-Garibay, *J. Org. Chem.* **2013**, *78*, 5293.

[16] a) W. Setaka, S. Ohmizu, C. Kabuto, M. Kira, *Chem. Lett.* **2007**, *36*, 1076; b) W. Setaka, S. Ohmizu, M. Kira, *Chem. Lett.* **2010**, *39*, 468; c) W. Setaka, K. Yamaguchi, *J. Am. Chem. Soc.* **2012**, *134*, 12458; d) W. Setaka, K. Yamaguchi, *Proc. Natl. Acad. Sci. USA* **2012**, *109*, 9271; e) W. Setaka, A. Koyama, K. Yamaguchi, *Org. Lett.* **2013**, *15*, 5092.

[17] See also N. S. Khan, J. M. Perez-Aguilar, T. Kaufmann, P. A. Hill, O. Taratula, O.-S. Lee, P. J. Carroll, J. G. Saven, I. J. Dmochowski, *J. Org. Chem.* **2011**, *76*, 1418.

[18] A. J. Nawara-Hultzsch, Doctoral Dissertation, Universität Erlangen-Nürnberg, **2008**; the crystallographic data for certain complexes have been further refined since this dissertation, so some values reported herein differ slightly.

[19] A. J. Nawara-Hultzsch, K. Skopek, T. Shima, M. Barbasiewicz, G. D. Hess, D. Skaper, J. A. Gladysz, *Z. Naturforsch. B* **2010**, *65*, 414.

[20] A figure is provided in the Supporting Information.

[21] a) $^{31}P\{^{1}H\}$ NMR spectra at this stage showed several peaks.[20] Note that *Z/Z/Z*, *Z/Z/E*, *Z/E/E*, and *E/E/E* C=C isomers are possible for the intermediate tris(alkenes)in Scheme 2; b) when the filtrates were taken to dryness, the yields of crude cyclized products were typically 85–45%.

[22] S. O. Grim, R. L. Keiter, W. McFarlane, *Inorg. Chem.* **1967**, *6*, 1133.

[23] W. H. Hersh, *J. Chem. Educ.* **1997**, *74*, 1485: the *J* values given represent the apparent coupling between adjacent peaks of the triplet.

[24] J. S. Siegel, F. A. L. Anet, *J. Org. Chem.* **1988**, *53*, 2629.

[25] A reviewer questioned whether these data were correctly presented. Given the workup conditions, the isolated yields of *trans*-**13c** and *trans*-**14c** (28 and 20%, respectively) should not be regarded as reflecting that one isomer may be major/minor. With time, the 50:50 mixture observed spectroscopically becomes biased in favor of *trans*-**14c**.

[26] a) D. W. Meek, P. E. Nicpon, V. I. Meek, *J. Am. Chem. Soc.* **1970**, *92*, 5351; b) R. R. Cooke, J. L. Burmeister, *J. Organomet. Chem.* **1973**, *63*, 471; c) Y. S. Wong, S. Jacobson, P. C. Chieh, A. Carty, *Inorg. Chem.* **1974**, *13*, 284.

[27] This could be confirmed crystallographically, but the bent SCN and approximately linear NCS ligands were disordered.

[28] G. J. Palenik, M. Mathew, W. L. Steffen, G. Beran, *J. Am. Chem. Soc.* **1975**, *97*, 1059.

[29] As is often the case with such complexes, the ^{13}C NMR spectra did not exhibit SCN signals; one would have been expected for *trans*-**13c**, and two for *trans*-**14c**.

[30] M. Stollenz, M. Barbasiewicz, A. J. Nawara-Hultzsch, T. Fiedler, R. Laddusaw, N. Bhuvanesh, J. A. Gladysz, *Angew. Chem.* **2011**, *123*, 6777; *Angew. Chem. Int. Ed.* **2011**, *50*, 6647.

[31] M. Stollenz, N. Bhuvanesh, J. H. Reibenspies, J. A. Gladysz, *Organometallics* **2011**, *30*, 6510.

[32] E. B. Bauer, T. Shima, unpublished results, Universität Erlangen-Nürnberg.

[33] E. B. Bauer, F. Hampel, J. A. Gladysz, *Organometallics* **2003**, *22*, 5567.

[34] a) G. D. Hess, Doctoral Dissertation, Universität Erlangen-Nürnberg, **2010**; b) T. Fiedler, Doctoral Dissertation, Universität Erlangen-Nürnberg, **2011**.

[35] T. Shima, E. B. Bauer, F. Hampel, J. A. Gladysz, *Dalton Trans.* **2004**, 1012. The product/catalyst system in reference [19] therein rapidly attains monomer/oligomer equilibrium, which can be reversibly varied as a function of concentration.

[36] a) J. C. Conrad, M. D. Eelman, J. A. Duarte Silva, S. Monfette, H. H. Parnas, J. L. Snelgrove, D. E. Fogg, *J. Am. Chem. Soc.* **2007**, *129*, 1024; b) S. Monfette, D. E. Fogg, *Chem. Rev.* **2009**, *109*, 3783.

[37] Representative structures: a) *trans*-$[MCl_2(P(iPr)(tBu)_2)_2]$ (M = Pd, Pt): C. M. DiMeglio, K. J. Ahmend, L. A. Luck, E. E. Weltin, A. L. Rheingold, C. H. Bushweller, *J. Phys. Chem.* **1992**, *96*, 8765; b) *trans*-$[PdBr_2(PCy_3)_2]$: M. L. Clarke, A. G. Orpen, P. G. Pringle, E. Turley, *Dalton Trans.* **2003**, 4393; c) *trans*-$[PtBr_2(PEt_3)_2]$: G. G. Messmer, E. L. Amma, *Inorg. Chem.* **1966**, *5*, 1775; d) *trans*-$[PdI_2(PEt_3)_2]$: R. Fränkel, J. Kinczek, H. Poniewar, H. Nöth, K. Polbrom, W. P. F. Fehlhammer, *Inorg. Chim. Acta* **2001**, *312*, 23; e) *trans*-$[PtBr_2(PCy_3)_2]$: T. S. Cameron, H. C. Clark, A. Linden, A. M. Nicholas, *Polyhedron* **1990**, *9*, 1683; f) *trans*-$[MI_2(PCy_3)_2]$ (M = Pd, Pt): N. W. Alcock, P. G. Leviston, *J. Chem. Soc. Dalton Trans.* **1974**, 1834.

[38] A. Bondi, *J. Phys. Chem.* **1964**, *68*, 441.

[39] The van der Waals radius of an sp hybridized nitrogen atom, 1.55 Å, is added to the average metal–nitrogen distances in the following complexes: a) *trans*-$[Pt(CN)_2(PCy_3)_2]$: B.-H. Xia, C.-M. Che, D. L. Phillips, K.-H. Leung, K.-K. Cheung, *Inorg. Chem.* **2002**, *41*, 3866; b) *trans*-$[Pd(CN)_2\{P(CH_2Ph)_3\}_2]$: B. Bendiksen, W. C. Riley, M. W. Babich, J. H. Nelson, R. A. Jacobson, *Inorg. Chim. Acta* **1982**, *57*, 29.

[40] a) E. V. Ansyln, D. A. Dougherty, *Modern Physical Organic Chemistry*, University Science Books, Sausalito, **2006**, pp. 97–98; b) E. N. Eliel, S. H. Wilen, *Stereochemistry of Organic Compounds*, Wiley, Hoboken; **1994**, pp. 624–629 and 1142–1155.

[41] This voluminous literature is easily accessed via the usual search engines; see for example F. E. Udwadia, B. Han, *J. Appl. Mech.* **2008**, *75*, 021011.

[42] D. Skaper, Doctoral Dissertation, Universität Erlangen-Nürnberg, **2010**.

[43] E. B. Bauer, F. Hampel, J. A. Gladysz, *Adv. Synth. Catal.* **2004**, *346*, 812.

[44] a) R. D. Horansky, L. I. Clarke, J. C. Price, T.-A. V. Khuong, P. D. Jarowski, M. A. Garcia-Garibay, *Phys. Rev. B* **2005**, *72*, 014302; b) R. D. Horansky, L. I. Clarke, E. B. Winston, J. C. Price, S. D. Karlen, P. D. Jarowski, R. Santillan, M. A. Garcia-Garibay, *Phys. Rev. B* **2006**, *74*, 054306.

[45] H. K. Cammenga, M. Epple, *Angew. Chem.* **1995**, *107*, 1284; *Angew. Chem. Int. Ed. Engl.* **1995**, *34*, 1171; the T_e values best represent the temperature of the phase transition or endotherm. DSC measurements were generally not continued above the initial mass loss temperature (TGA).

[46] The slow addition of the Grubbs' catalyst at 0 °C is essential; otherwise the proportion of oligomeric products increases substantially.

[47] The ^{1}H and ^{13}C NMR assignments were made by $^{1}H,^{1}H$ COSY and $^{1}H,^{13}C\{^{1}H\}$ COSY spectra.

[48] This coupling represents a satellite (d, $^{195}Pt = 33.8\%$) and is not reflected in the peak multiplicity given.

[49] *m/z* (relative intensity,%); the most intense peak of isotope envelope is given; FAB, 3-NBA; ESI(+).

[50] The microanalytical data are not in good agreement with this spectroscopically pure sample, but are reported to illustrate the best result obtained. The ^{1}H and $^{13}C\{^{1}H\}$ NMR spectra of **19** are provided in the supporting information.

[51] The ^{1}H and ^{13}C NMR assignments were made by analogy to *trans*-**4c**.

[52] The total mmol was calculated from the mass using the product ratios found by $^{31}P\{^{1}H\}$ NMR.

[53] The phenyl protons were assigned by a $^{1}H,^{1}H$ COSY NMR spectrum.

[54] The *i*-Ph ^{13}C signal was not observed.

Received: November 12, 2013
Published online on March 6, 2014